SRC TR 86-34

A Biophysical Model of Cochlear Processing: Intensity Dependence of Pure Tone Responses

by

S.A. Shamma, R.S. Chadwick, W. John Wilbur, K.A. Morrish, and J. Rinzel

A biophysical model of cochlear processing: Intensity dependence of pure tone responses

Shihab A. Shamma,[a] Richard S. Chadwick,[b] W. John Wilbur, Kathleen A. Morrish, and John Rinzel
Mathematical Research Branch, National Institute of Arthritis, Diabetes, Digestive and Kidney Diseases, National Institutes of Health, Bethesda, Maryland 20892

(Received 17 September 1984; accepted for publication 11 February 1986)

A mathematical model of cochlear processing is developed to account for the nonlinear dependence of frequency selectivity on intensity in inner hair cell and auditory nerve fiber responses. The model describes the transformation from acoustic stimulus to intracellular hair cell potentials in the cochlea. It incorporates a linear formulation of basilar membrane mechanics and subtectorial fluid–cilia displacement coupling, and a simplified description of the inner hair cell nonlinear transduction process. The analysis at this stage is restricted to low-frequency single tones. The computed responses to single tone inputs exhibit the experimentally observed nonlinear effects of increasing intensity such as the increase in the bandwidth of frequency selectivity and the downward shift of the best frequency. In the model, the first effect is primarily due to the saturating effect of the hair cell nonlinearity. The second results from the combined effects of both the nonlinearity and of the inner hair cell low-pass transfer function. In contrast to these shifts along the frequency axis, the model does not exhibit intensity dependent shifts of the spatial location along the cochlea of the peak response for a given single tone. The observed shifts therefore do not contradict an intensity invariant tonotopic code.

PACS numbers: 43.63.Bq

INTRODUCTION

Nonlinearities in cochlear function have been the focus of extensive experimental and theoretical study. One such phenomenon concerns the nonlinear dependence of the frequency selectivity of phase locking on stimulus intensity in the auditory nerve to simple and complex sounds (Moller, 1983a; Evans, 1977; Smoorenburg and Linschoten, 1978). With increasing intensity, the selectivity of the response transfer function deteriorates and the frequency of best response shifts downwards. Recent intracellular recordings of ac transfer functions of inner hair cells in the apical cochlear region exhibit similar dependence on stimulus intensity (Dallos and Santos-Sacchi, 1983). Moller (1978) attributed these effects to nonlinear broadening and downward shift of basilar membrane tuning. Other investigators (Evans, 1977; Wilson and Evans, 1983), however, demonstrated linear tuning of the basilar membrane at these intensity levels, and concluded that the deterioration may be due to effects in the hypothetical "second filter" between the membrane and the hair cells. Despite these downward shifts of the best frequency, psychophysical experiments show relatively slight dependence of pitch perception on intensity for single tones (Wever, 1949; Moller, 1978) and none at all for complex tones (Terhardt, 1975). These apparent contradictions would raise serious doubts regarding the intensity invariance of the cochlear tonotopic map and its relevance for pitch coding in the auditory system. In this report, we address this issue and demonstrate that a specific theoretical model using linear basilar membrane mechanics and space-independent fluid–cilia coupling can account for these intensity effects and yet maintain an intensity invariant tonotopic map.

A major part of our effort here involves developing a composite model of the various cochlear stages that is efficient to compute and is founded on basic principles and experimental data from the different constituents of the peripheral auditory system. We use the model to demonstrate the contribution of the various stages to the nonlinear intensity-dependent changes of the frequency tuning curves and other input/output measures of the response to single low-frequency tones.

A schematic of the basic building blocks of the model and their amplitude transfer characteristics is shown in Fig. 1. It is worth reiterating that these transfer characteristics are based on computations using mostly explicit biophysical parameters discussed in later sections and are not assumed *a priori*. The first stage is a linear, three-dimensional model of basilar membrane mechanics which incorporates basic physiological parameters in its formulation (Chadwick and Cole, 1979; Chadwick *et al.*, 1980). The present treatment is primarily valid for the low-frequency range (< 1500 Hz). At a given location along the cochlea the mechanical transfer function describes the ratio of basilar membrane displacement to stapes displacement as a function of stimulus frequency (i.e., the frequency tuning curve at that location). The basilar membrane displacement then produces an inner hair cell cilia displacement via the second block, which includes coupling of the cilia to the fluid in the subtectorial space. This stage exhibits the experimentally observed high-

[a] Present address: Electrical Engineering Department, University of Maryland, College Park, MD 20742.
[b] Present address: Biomedical Engineering and Instrumentation Branch, Division of Research Services, National Institutes of Health, Bethesda, MD 20892.

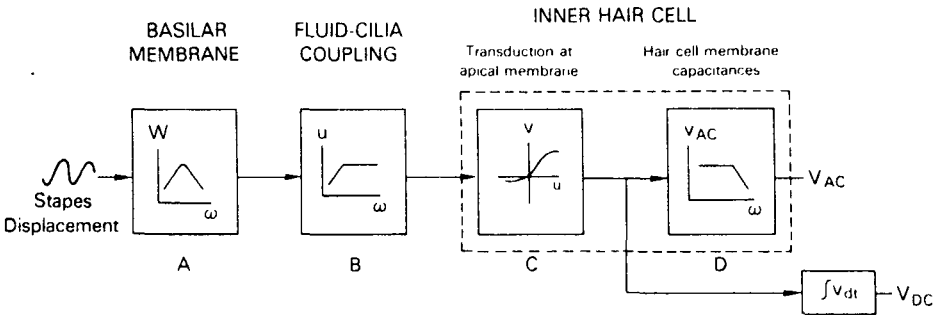

FIG. 1. Simplified block diagram of the processing stages of the composite cochlear model.

pass ("velocity") transfer function and assumes space-independent parameters (i.e., identical hair cell characteristics and cilia lengths). Our model for inner hair cell electrical activity is based on a simplified description of the anatomy and electrophysiology of the organ of Corti and on experimental studies of the nonlinear mechanisms of the hair cell ciliary transduction (Corey and Hudspeth, 1983a; Dallos, 1983; Russell and Sellick, 1978; Russell, 1983). Under certain assumptions its transfer characteristics can be subdivided into two elements: (1) The saturating, asymmetric, nonlinear transduction of cilia displacement into conductance changes of the apical membrane, which results in modulations of hair cell currents and of the intracellular potentials and (2) the capacitive effects of the hair cell membrane which attenuate the ac potentials at high frequencies. The final outputs computed from the model are the peak-to-peak value of the inner hair cell potential (an ac measure) and its average value (a dc measure). These measures are discussed with reference to experimentally recorded hair cell potentials as functions of frequency and intensity.

In Secs. I and II we develop the various stages of the model and discuss in detail the limitations of the assumptions and approximations that allow a simple and intuitive formulation to emerge. In Sec. III we present the computed responses of the model as functions of the frequency and intensity of a single tone. Finally, these results are analyzed in Sec. IV in light of the published data and certain conclusions regarding cochlear processing and neural encoding of sound are discussed.

I. COCHLEAR MECHANICS AND FLUID–CILIA COUPLING

A. Basilar membrane motion

The basilar membrane model has been discussed elsewhere (Chadwick and Cole, 1979; Chadwick *et al.*, 1980; Chadwick, 1985). The intent here is to summarize the essential ideas and approximations used in the model. The equations used to calculate the basilar membrane motion are given in the Appendix. The system consists of a slender, coiled, rigid tube having a variable cross-sectional area that is filled with a viscous, incompressible fluid. The tube is divided lengthwise into two chambers (scala vestibuli, scala tympani) by an interior surface, part of which is rigid and part viscoelastic (basilar membrane). The viscoelastic portion is a highly anisotropic plate having variable width and thickness, and a damping per unit area proportional to basilar membrane velocity. The system is driven by a prescribed pure tone stapes displacement at the basal end of the tube. At the apical end, pressure is equalized at the helicotrema. The plate deflects due to the pressure difference across it in the fluid, and the fluid motion is coupled locally to the plate motion. A sketch of the uncoiled model is shown in Fig. 2(a). The theory applies to the actual coiled geometry, however. All geometrical parameters in the model are chosen consistent with anatomical data for the guinea pig (Fernandez, 1952).

Amplitudes are assumed to be small enough that linearization of the hydrodynamics and elasticity should be a good approximation. In the present formulation the antisymmetric saturating nonlinearity of the hair cell conductance is taken to be the dominant nonlinearity (cf. Sec. IV). Furthermore, our solution methods here apply to the low-frequency end (< 1500 Hz) of the auditory range, where specialized asymptotics simplify the calculations. The resulting theory involves the three-dimensional motion of the fluid and can be shown to be a low-frequency limit of Holmes and Cole, 1984.

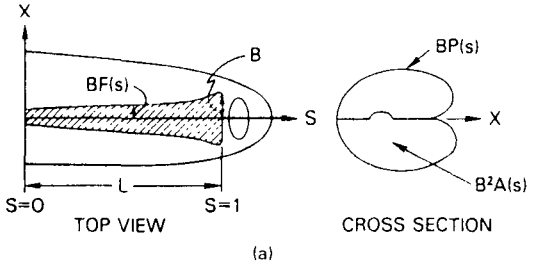

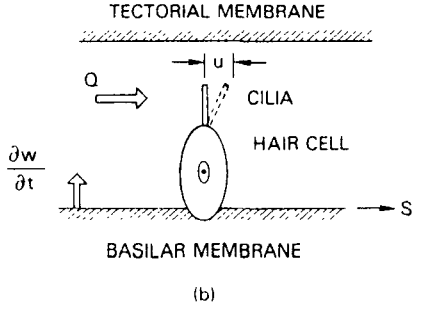

FIG. 2. (a) Top view and cross section of the basilar membrane model (see text, Appendix, and Table I for function definitions). (b) Schematic of fluid–cilia coupling stage. w = basilar membrane displacment, Q = fluid velocity, u = cilia displacement.

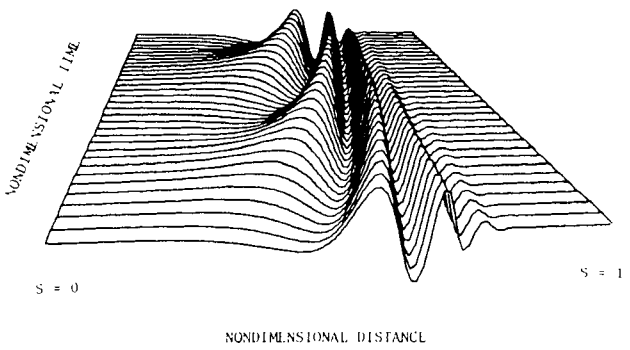

FIG. 3. Traveling wave displacement of basilar membrane model as a function of time and distance along the cochlea. Two periods are shown. The stimulus is a pure tone at 700 Hz; the parameters are those of Table I.

The nature of the computed basilar membrane waveform is shown in Fig. 3, where a perspective view of the center line plate deflection ($x = 0$) is plotted as a function of spatial location (s increasing from left to right) and time (increasing away from observer). Several features of the traveling wave are notable: The wavelength decreases, the phase velocity decreases, and the amplitude increases as the region of maximal response is approached. Both forward and reflected waves are included in the solution [cf. Eq. (A1)], but in this particular example at 700 Hz the reflected wave contribution to the response is negligible. At lower frequencies the reflected wave amplitude becomes larger. [A tuning curve for $s = 0.65$ is shown in Fig. 7(a).] The frequency of best response, 615 Hz, and the high-frequency slope, 31 dB/oct, both obtained at $s = 0.65$, are consistent with low-frequency experimental data (von Békésy, 1960) for the guinea pig. Note that the high-frequency slope is computed by performing a linear regression on all computed points between 6 and 12 dB below peak (Morrish *et al.*, 1986).

B. Fluid–cilia coupling

In contrast to outer hair cells, which are thought to be driven directly by the displacement of the basilar membrane, inner hair cells are not imbedded in the tectorial membrane, and so they instead must be driven by fluid motion. There is anatomical and electrophysical support for this hypothesis. For instance, tuning curves for intracellular recordings from inner hair cells exhibit low-frequency slopes that are 6 dB/oct steeper than those obtained from the outer hair cells (Dallos and Santos-Sacchi, 1983). To account for this effect, the following simple model is proposed [see Fig. 2(b)]. Let u be some measure of displacement of the inner hair cell cilia, e.g., linear displacement of the bundle tip or angular displacement at the root; u is the mechanical input to the hair cell model. We seek to find a relationship between u and basilar membrane displacement w. For the present discussion we can ignore the details of the velocity field distorting the cilia bundle, and simply refer to some spatial mean of the transverse component Q. Because of linearity, Q will be proportional to $\partial w/\partial t$, and the constant of proportionality depends on the geometry of the space between the apical surface of the hair cells and the tectorial membrane. Since the subtectorial gap is small, the Reynolds' number is small, and therefore the force deflecting the bundle will be proportional to the fluid velocity Q. The constant of proportionality depends on the geometry of the bundle and the viscosity of the endolymph. Resisting this deflecting force are an elastic force proportional to u and a dissipative force proportional to $\partial u/\partial t$. Since the individual cilia apparently behave like rigid rods and do not bend (Flock and Strelioff, 1984), the elastic force is due to an effective torsional spring at the base of the cilia bundle, and the dissipation is caused by the material holding together the bundle and perhaps internal dissipation in the individual cilia. These arguments then lead to the relation connecting w and u:

$$\tau_c \frac{\partial u}{\partial t} + u = \tau_c C \frac{\partial w}{\partial t}. \tag{1}$$

For simple harmonic motion this gives the transfer function

$$u/w = Ci\Omega\tau_c/(1 + i\Omega\tau_c). \tag{2}$$

The two constants in Eq. (2), the gain C and time constant τ_c, depend on the abovementioned proportionality relations. A sketch of the magnitude of the transfer function [Fig. 1(b)] shows its high-pass characteristics. The hair cell here is driven by velocity up to frequency ($1/2\pi\tau_c$) and by displacement beyond that. This pole primarily accounts for the apparent disappearance at higher frequencies (> 500–900 Hz) of a 90° phase lead between the inner and outer hair cell potentials (Dallos and Santos-Sacchi, 1983; Sellick and Russell, 1980; Sellick *et al.*, 1982). Alternative formulations have been advanced to deal with this issue (Dallos and Santos-Sacchi, 1983), but definitive experimental evidence is lacking at present (Sellick *et al.*, 1982). It should be noted, however, that the qualitative features of the computed magnitude transfer functions are relatively intensitive to τ_c. The transfer function of Eq. (2) has a gain $C(= 0.1)$ such that stapes displacements and corresponding cilia displacements and transduced hair cell potentials are all within physiologic ranges. Finally, note that this coupling is independent of position along the cochlea and hence is unlike the hypothetical "second filter" proposed by several investigators (e.g., Allen, 1980). A possible generalization of our present mode is to include an s-dependent cilia length which is observed in some species (Weiss, 1984), which would affect the time constant τ_c. In this case, τ_c is proportional to cilia length (l) since the viscous force varies directly with l, while the elastic restoring force (which is lumped at the cilia base) is independent of l.

II. INNER HAIR CELL DISPLACEMENT–VOLTAGE TRANSDUCTION

A. Hair cell model

In this section we develop and analyze a hair cell model based on experimental measurements of intracellular recordings in the hair cell of the guinea pig [(Dallos and Santos-Sacchi, 1983; Russell and Sellick, 1978) *in vivo*] and of the bullfrog sacculus [(Corey and Hudspeth, 1983a) *in vitro*]. We first derive a mathematical description of this model, then discuss assumptions and parameter considerations, and finally exploit several approximations that allow a simple and accurate description of the hair cell transfer charac-

teristics in both the linear and nonlinear regimes.

Our starting point is a somewhat simplified version of hair cell–epithelium equivalent circuit proposed by Cory and Hudspeth (1983a) (Fig. 4). It is in essence similar to the circuit of the "resistance microphonic" theory proposed in Davis (1965). In our circuit, only those components affecting the behavior of the intracellular potential responses are preserved. By applying Kirchoff 's current law to the equivalent circuit of Fig. 4, we derive an equation relating the intracellular hair cell potential V to the cilia displacement u:

$$(C_a + C_b)\frac{dV}{dt} + G(u)(V - E_t) + G_K(V - E'_K) = 0. \tag{3}$$

Here E_t is the endocochlear potential (Dallos, 1973) and $E'_K \approx E_K + E_t R_p/(R_t + R_p)$, where E_K is the reversal potential for ionic current [primarily dominated by K^+ (Lewis and Hudspeth, 1983; Corey and Hudspeth, 1983a)] across the basal membrane of the hair cell, here slightly corrected to E'_K to account for the extracellular pathway (shown dashed in Fig. 4) which sets up a nonzero extracellular resting potential near the basal membrane of the hair cell.

The resistance of the pathway through the hair cell membrane from the endolymph of the scala media to the perilymph of the scala tympani is much larger than that through the leaky epithelium, i.e., $1/R_t \gg G, G_k$ (Corey and Hudspeth, 1983a). (Similarly, the hair cell membrane capacitances greatly exceed the epithelial capacitance; therefore, the latter are not shown in Fig. 4.) As a consequence the extracellular potential remains essentially constant and we treat it as such in our model. The hair cell is thus decoupled from the epithelial circuit and neighboring hair cells. Perturbations of intracellular potential and of the trans-baso-lateral membrane potential become equivalent. These observations are consistent with experimental findings (Dallos, 1983). Furthermore, we assume that all the hair cell intracellular fluid space is equipotential and thus can be represented by a single node (Dallos, 1983).

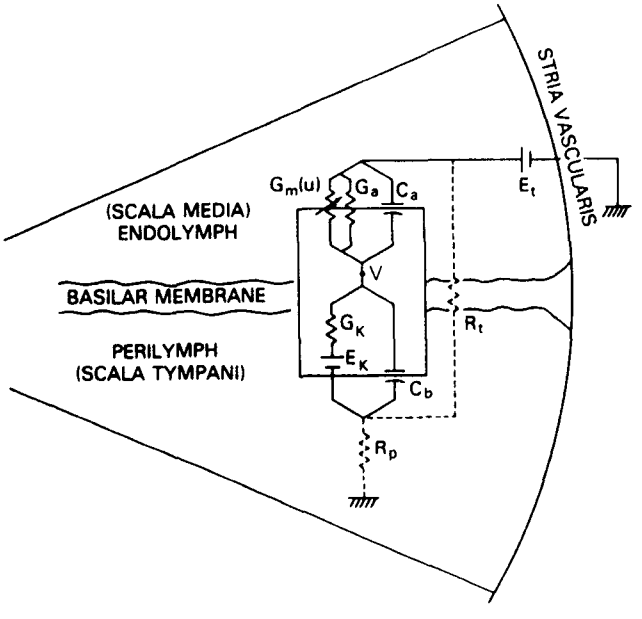

FIG. 4. Schematic diagram of a radial section of the cochlea, including the equivalent circuit of the inner hair cell and surrounding structures. E_t = endocochlear potential; R_t, R_p = epithelium resistances; E_K = potassium reversal potential; G_K = ionic channel conductance of the hair cell basal membrane; $G_m(u)$ = mechanically sensitive conductance of the hair cell apical membrane; G_a = leakage conductance of the hair cell apical membrane; u = cilia displacement; V = hair cell intracellular potential.

In this circuit we have retained only the primary contributions to membrane conductance: a conductance $G(u)$ in the apical portion[1] of the hair cell which includes a mechanically sensitive non-ion-selective transducer channel, and a K^+-dominated conductance (G_K) in the basal membrane. While several voltage-dependent ionic channels (K^+, Ca^{++}) are at present being investigated in vertebrate hair cells (Lewis and Hudspeth, 1983; Corey and Hudspeth, 1983b) (time constants 0.4–80 ms), relatively little information is available about such channels in mammalian hair cells. For this reason, and to keep our model simple, we here assume that G_K and $G(u)$ are not voltage dependent: G_K remains at its steady-state value (1.07×10^{-8} S). This value and the resting apical membrane resistance G_0 [$= G(0)$] are chosen to give a total steady-state hair cell resistance [$1/(G_0 + G_K)$] of 66 MΩ (Russell and Sellick, 1978) and a rest potential of approximately -28.4 mV (Russell and Sellick, 1978; Dallos and Santos-Sacchi, 1983).

The conductance of the apical membrane is the sum of a mechanically sensitive term $G_m(u)$ and a constant (leakage) term (Hudspeth and Corey, 1977; Russell and Sellick, 1978; Dallos, 1983). For the mechanically varying part we employ the direct coupling model proposed by Corey and Hudspeth (1983a) in their analysis of the bullfrog saccular hair cell. In this view, cilia displacement activates ionic channels directly rather than via chemical mediators. Experimental evidence suggests that the time constants (order of μs) for activation–inactivation processes are much shorter than the time scales of frequencies (< 1500 Hz) considered here (Corey and Hudspeth, 1983b). This allows the use of the Boltzmann distribution to represent the distribution of channel states as an instantaneous function of u. We may write the total mechanically sensitive conductance as the product of G_{max}, the conductance with all channels fully open, and $P_c(u)$, the fraction of channels in the open state. We determine P_c according to the Boltzmann distribution and assume a channel model with two states (open and closed) so that

$$G_m(u) = G_{max} P_c(u) = G_{max}/[1 + \exp(\Delta G_{act}/RT)], \tag{4}$$

where ΔG_{act} is the channel activation energy. Here ΔG_{act} is modeled simply as a linear function of displacement $\Delta G_{act} = G_1 - Z_1 u$. Note that G_m is partially activated at zero displacement but inactivates completely for large negative displacement. As Hudspeth and Corey (1977) point out, this description of conductance is analogous to that for an instantaneous voltage-activated channel in excitable nerve membrane. These authors also describe and utilize a three-state model which allows a more precise fit of their data, but for our purposes the qualitative features are adequately provided by the two-state theory. The values of G_1 and Z_1 that we use in our model are close to those used by Corey and

Hudspeth (1983a); G_{max} is chosen so that the total change in apical membrane resistance under maximum displacement is approximately 25% (Hudspeth and Corey, 1977; Dallos, 1983).

All the numerical results discussed in Sec. III are generated using Eq. (3). However, a further simplification of this equation allows easy and intuitive understanding of these results. By rewriting $G(u) = G_0 + \tilde{G}(u)$, we define $\tilde{G}(u)$ as the modulation of the conductance due to the cilia displacement. Similarly, we write $V = V_0 + \tilde{V}$, where V_0 is the intracellular resting potential and $\tilde{V}$ is the potential deviation from rest. For parameter values under consideration here we find that $\tilde{G}$ is sufficiently small relative to the total resting conductance $G_0 + G_K$ so that $\tilde{V}$ is small compared to $E_t - V_0$, the driving potential (relative to rest) for the displacement-activated conductance. Hence we can make the approximation $E_t - V \simeq E_t - V_0$. Then by introducing dimensionless variables, Eq. (3) reduces to:

$$\tau \frac{dv}{dt} v = \tilde{g}(u), \tag{5}$$

where $\tau = (C_a + C_b)/(G_0 + G_k)$, $v = \tilde{V}(G_0 + G_k)/[\beta G_{max}(E_t - V_0)]$, $\tilde{g} = \tilde{G}/\beta G_{max}$, $V_0 = (G_0 E_t + G_k E_k')/(G_0 + G_k)$, and $\beta = \exp(-G_1/RT)$.

The hair cell then appears as a first-order low-pass filter with time constant τ. The "driving" term $\tilde{g}(u)$ is the result of nonlinear transduction from cilia displacement $u(t)$ to ionic conductance. The "output" potential v is the result of low-pass filtering the driving waveform. (See Fig. 1.)

B. Hair cell transfer characteristics

Figure 5(a) shows the intracellular potential V in response to a sinusoidal input function $u(t) = u_0 \sin(\omega t)$, applied at various amplitudes u_0. At the lowest amplitudes, the intracellular potential is sinusoidal and is linearly related to $u(t)$. At higher amplitudes, however, the effect of the saturating transducer nonlinearity becomes progressively larger. The troughs of the voltage waveforms saturate first [because of the asymmetry in $\tilde{g}(u)$], followed at higher amplitudes by the crests. In Fig. 5(b) the hair cell potential for a fixed amplitude u_0 is plotted over one period of the response for three different frequencies. The changes in the waveform with increasing frequency are due to the attenuation of the ac components by the hair cell membrane capacitances.

There are two distinct types of experimental measures of these waveforms that have been widely used. One is an *average* measure, which is the average value of the potential (deviation from rest) over one period. This measure increases for higher input amplitudes because of the increasing asymmetry in the waveform. It is therefore a direct consequence of the asymmetry in the transducer nonlinearity. Because this average evaluates the time-independent Fourier component in the waveform, we call it the dc measure. The second type of measure takes into account the *temporal* changes in the waveform over a period. One such measure is the peak-to-peak value; another is the amplitude of the first Fourier harmonic. Note that the deformed output waveform is not a pure sinusoid and hence contains several harmonics of the input frequency. We shall use the peak-to-peak value of the waveform as the ac measure. This measure is relatively easy to obtain experimentally and numerically, but is theoretically a complicated measure of all the harmonics.

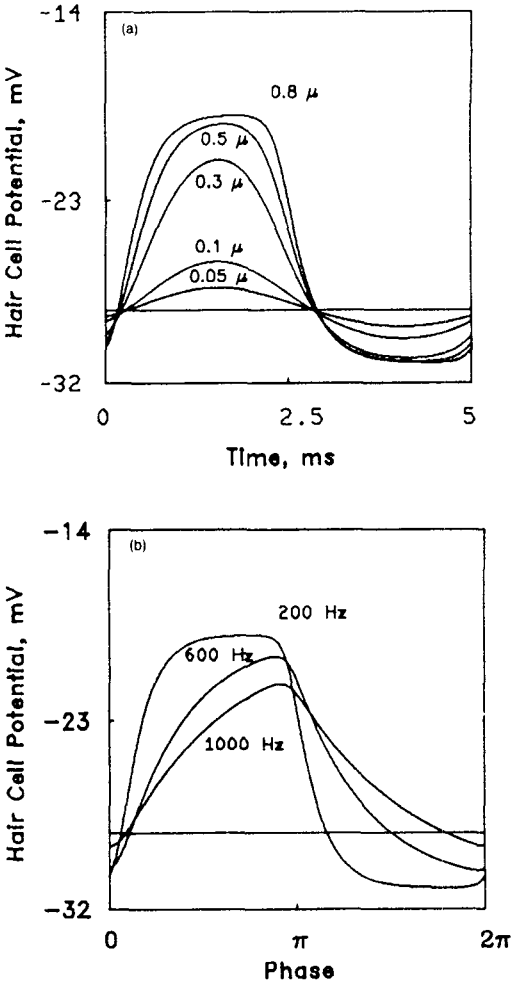

FIG. 5. (a) Waveform of hair cell intracellular potential in response to sinusoidal cilia displacement function $u(t) = u_0 \sin \omega_0 t$, where $\omega_0/2\pi = 200$ Hz and cilia displacement u_0 is the parameter. (b) Waveform of hair cell intracellular potential plotted versus phase over one period in response to sinusoidal displacement function $u(t) = u_0 \sin \omega t$, where cilia displacement $u_0 = 1\ \mu$m, and frequency $\omega/2\pi$ is the parameter.

1. Frequency responses—ac measures

Many investigators describe the transfer characteristics of a hair cell by its response as a function of the frequency of a constant amplitude sinusoidal input, i.e., by a "transfer function" (Corey and Hudspeth, 1983a; Dallos and Santos-Sacchi, 1983). This is convenient for the *in vivo* experiments where single tone stimuli are used. Also, such data are most easily interpretable for the linear regime of low tone intensity. However, for our theoretical model of Eq. (3) there are no simple correspondences between the input and output frequencies because the output $v(t)$ depends nonlinearly upon the input $u(t)$. It is, however, possible to predict the qualitative behavior of output ac measures based on the simplification of Eq. (5). For example, consider a sinusoidal cilia displacement $u(t) = u_0 \sin(\omega_0 t)$ of constant amplitude

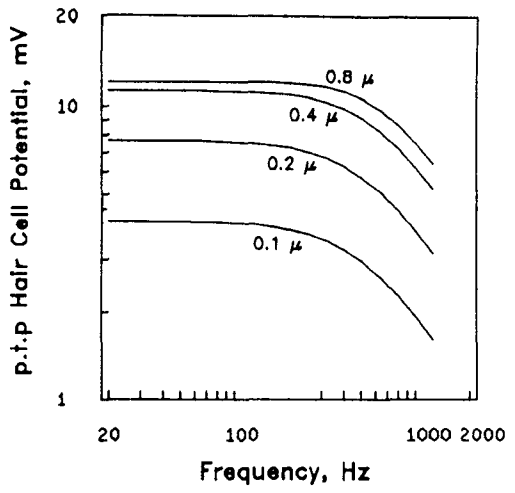

FIG. 6. Hair cell ac transfer characteristics. Each curve represents the peak-to-peak intracellular potential versus frequency of sinusoidal displacement presented at a certain maximum cilia displacement level (indicated by the associated parameter).

u_0. The nonlinearity $\tilde{g}(u)$ deforms $u(t)$ and results in a waveform composed of a dc term and several harmonics (the largest of which is the first harmonic). The output of the system v is then the superposition of these components, each acted upon separately by the same linear low-pass filter. Therefore, in sweeping the input frequency, *any ac measure of the output* will display a low-pass function of frequency. This is illustrated in Fig. 6, where each curve represents the peak-to-peak value of the potential [computed from Eq. (3)] plotted versus the frequency of a constant amplitude sinusoid. The effect of the saturating nonlinearity $\tilde{g}(u)$ is manifested in the "bunching up" of the curves at larger u_0 (output curves for $u_0 > 0.7$ μ cannot be easily distinguished).

2. Frequency responses—dc measures

Unlike the ac components, the dc measure is independent of the input frequency. This is precisely true for Eq. (5) and a good approximation for Eq. (3). At high frequencies ($\geq \frac{1}{2}\pi\tau$) the dc measure is the only surviving part in the response because the ac components attenuate drastically.

III. RESPONSE OF THE COMPOSITE MODEL TO SINGLE TONE STIMULI

Representative calculations will now be presented that show how a pure tone introduced at the stapes is transformed into intracellular potentials of inner hair cells. For fixed geometrical, mechanical, and electrical parameters in the model (see Table I),[2] the hair cell response depends on the frequency of the tone, the stapes amplitude, and the distance of the hair cell from the stapes. In this section we fix the distance at $s = 0.65$; the effects of location will be discussed in Sec. IV. We characterize the cochlear transformation in two ways. First, we determine the frequency dependence of the response with stapes amplitude as a parameter; Fig. 7(b) and (c) shows such isointensity plots of the inner hair cell potential for both ac and dc measures. Second, we compute

TABLE I. Parameter values.

$L = 1.85$ cm
$B = 0.0125$ cm
$\nu = 0.008$ cm^2/s
$D_0 = 0.094$ dyn/cm
$\rho = 1$ g/cm^3
$A(s) = 2h^2$
$F(s) = (8 + 5s)/13$
$P(s) = 6h$
$D(s) = h^3$
$h_0 = 0.0007$ cm
$h = 1 \quad s < 0.2$
$0.1 + 0.9\exp(0.7-3.5s), \quad s > 0.2$
$H = 6.5 - 17s, \quad s < 0.176$
$= 3.8 - 1.7s, \quad s > 0.176$
$C' = 115$ dyn/cm^3
$M = 3$
$C = 0.1$
$\tau_c = 0.3$ ms
$E_t = 100$ mV
$E_k = -84$ mV
$R_p/(R_p + R_t) = 0.04$
$C_a + C_b =$ pF
$G_k = 1.07 \times 10^{-8}$ S
$G_{max} = 0.15 \times 10^{-8}$ S
$G_0 = 0.43 \times 10^{-8}$ S
$Z_t/RT = 10\mu m^{-1}$
$\exp(-G_t/RT) = 0.25$

the ac and dc hair cell potential versus stapes amplitude with frequency as a parameter; Fig. 8(a) and (b) illustrates these functions. We will first discuss these numerical results (Figs. 7 and 8) in terms of the processing of a cascade of filters, with reference to the functional diagram of Fig. 1. Then, in Sec. III B, we present analytical results based on the simplified hair cell equation (5) which give additional insights.

A. Numerical computations

The cilia displacement u is first determined using the analytical theory outlined in Sec. I. Equation (3) is then solved numerically as follows. The periodic response is computed directly and efficiently by first determining the initial conditions which eliminate the transient portions of the response. This is accomplished by writing the solution in terms of an integrating factor with definite integrals and one undetermined constant of integration which represents the initial condition (Boyce and Diprima, 1977). The definite integrals involved are computed numerically and the constant is then evaluated by requiring that the solution be periodic.

1. The ac responses

The peak-to-peak hair cell potential as a function of frequency exhibits significant changes for the different stapes amplitudes of Fig. 7(b). We first consider the changes in the isointensity response generated at each stage in the model (Fig. 1) and then discuss the effect of stapes amplitude on the final output.

The isointensity response of the basilar membrane [in

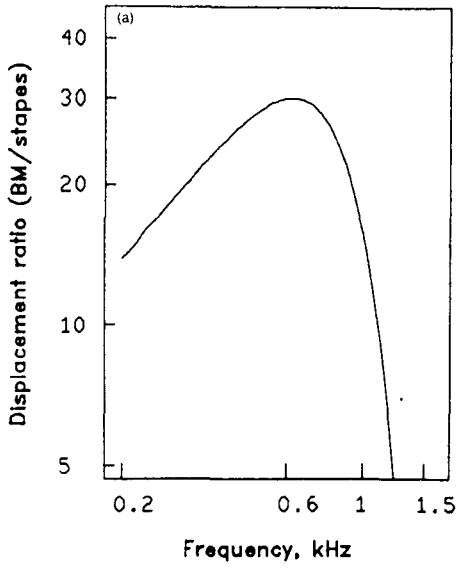

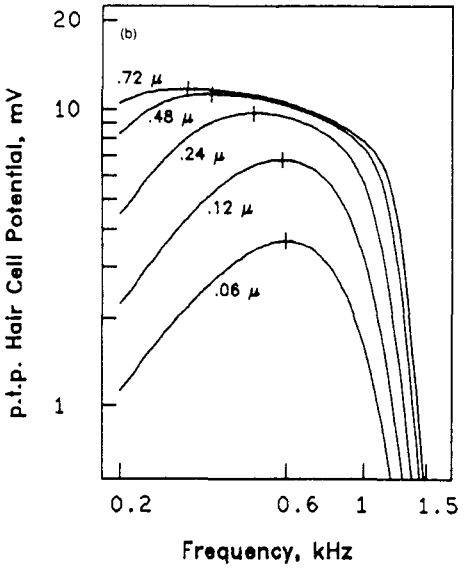

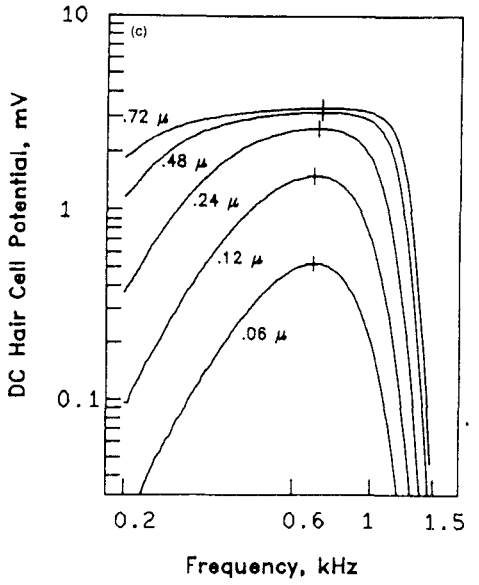

FIG. 7. (a) Peak basilar membrane displacement versus frequency at a constant stapes amplitude = 0.1 μm and a fixed location $s_0 = 0.65$. (b) ac transfer characteristics of the composite model. Each curve represents the peak-to-peak intracellular potential versus frequency of sinusoidal stapes displacement presented at a certain maximum displacement level (indicated by the associated parameter) and a fixed location $s_0 = 0.65$. (c) dc transfer characteristics of the composite model. Each curve represents the average intracellular potential (deviation from rest) versus frequency of sinusoidal stapes displacement presented at a certain maximum displacement level (indicated by the associated parameter) and a fixed location $s_0 = 0.65$.

Figs. 1(a) and 7(a)] is filtered by the transfer function of the fluid–cilia coupling stage which results in a steeper low-frequency slope and an upward shift in the frequency of the peak response.[3] These effects are expected to be larger in more apical hair cells (i.e., larger s) since their BF approaches that of the cutoff frequency of the fluid–cilia coupling filter stage (550 Hz) and the isointensity response of the basilar membrane becomes progressively less tuned. Because of *linear* basilar membrane mechanics and fluid–cilia coupling, this upward BF shift is independent of stapes amplitude. Amplitude dependence in the model is first exhibited at the next stage, in which the isointensity response of the cilia displacement is flattened by the hair cell saturating nonlinearity [Fig. 1(c)]. For large stapes amplitude a significant frequency range is affected and hence the response appears less tuned. The final stage is low-pass filtering [Fig. 1(d)] which steepens the high-frequency slope and shifts the BF downward. Note, however, that at significantly higher frequencies (> 3–4 kHz), where the basilar membrane frequency response is expected to be sharper, the downward BF shifts may decrease. The amount of downward shift increases with larger basilar membrane amplitudes as the hair cell response becomes more saturated and less tuned, especially for locations for which the BF lies in the frequency range where the low-pass slope is steepest.

There are then two sources for the BF shifts. The first is independent of stapes amplitude. It is attributable to the action of the linear cascade of filters (upwards by the high pass of the fluid–cilia coupling and downwards by the low pass of the hair cell). These BF shifts are influenced by the broadness of the basilar membrane tuning in the low-frequency region of the cochlea. They may be significantly reduced in this region if we include the overall effects of the middle ear low-pass filter (Flanagan, 1972) which further steepens the high-frequency slopes of the basilar membrane tuning curves beyond the 6-dB/oct slopes of the cascade of filters. The second source of BF shifts (on which we will concentrate in the remainder of this report) is nonlinear and is strongly dependent on the action of the hair cell saturating nonlinearity and low-pass filter. It manifests itself in the isointensity curves at higher amplitudes as downward BF shifts and increasing bandwidth of the response.

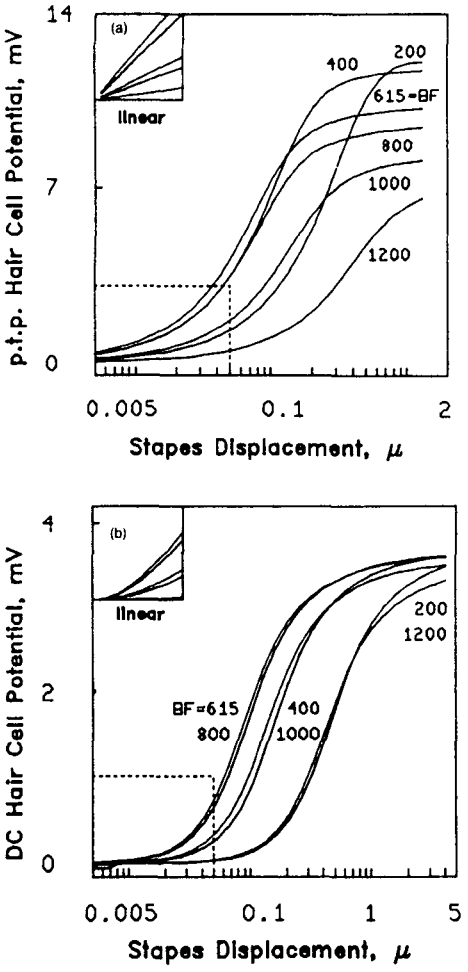

FIG. 8. (a) The ac hair cell potential (peak to peak) versus stapes displacement with frequency as a parameter. The inset is a replot with linear axes of the curve segments contained within the dashed box. It shows the linear dependence of the ac potential on stapes amplitude at low levels of intensity. (b) Average dc hair cell potential (deivation from rest) versus stapes displacement with frequency as a parameter. The inset is a replot with linear axes of the curve segments contained within the dashed box. It shows the quadratic dependence of the dc potential on stapes amplitude at low levels of intensity.

These amplitude-dependent changes of the response are shown in the computed ac responses of Fig. 7(b). At the highest intensity the frequency response between 200–1000 Hz [at Fig. 1(d)] is significantly saturated and appears almost flat to the hair cell low-pass filter; the overall ac response then resembles that filter's transfer function (Fig. 6).

A second characterization of the response is the ac response versus stapes amplitude with frequency as a parameter [Fig. 8(a)]. These ac functions show several features. The peak-to-peak level saturates and the level of saturation decreases with increasing frequency. This occurs because first the asymptotic (for large u) maximum and minimum values of hair cell conductance are limited by the saturating $g(u)$ and then the low-pass filter attenuates the ac output waveform more severely for higher frequencies. The BF curve is therefore the leftmost curve for small displacements but not for larger displacements.

2. The dc responses

There are significant differences between the ac and dc measures of hair cell output. First, because of the linearity of the basilar membrane model, the dc components in the response waveforms appear only *after* and as a result of the hair cell asymmetrical nonlinearity. The larger the basilar membrane displacement the more dc is generated. Second, the low-pass filter stage does not affect the dc measure. The dc outputs therefore do not show any downward shifts relative to basilar membrane BF, but rather upward shifts due to the fluid–cilia coupling. As in the case of the ac responses, this BF shift (relative to that of the basilar membrane) at small stapes amplitude is related to the broadness of the basilar membrane tuning curve. In the range of low intensities [where Eq. (5) is a good approximation] the BF remains fixed as intensity is varied. At higher intensities, however, the model solutions [computed from the more complete Eq. (3)] show some small upward shifts [Fig. 7(c)]. Note that the low-frequency slopes of the dc curves are steeper than the corresponding ac and basilar membrane curves (e.g., for the 0.06 μ maximum displacement curves, the slope of the ac curve is ≈ 13 dB/oct in the 200–400-Hz region, whereas the slope of the dc curve is ≈ 18 dB/oct); this sharpening effect is attributed to the hair cell nonlinearity (see the analytical results in Sec. III B).

In Fig. 8(b) the dc response is plotted versus stapes amplitude with frequency as a parameter. As in the ac case the BF curve is leftmost; here, this is true for almost the entire range of displacements. In addition, the saturating levels of these curves show relatively small dependence on frequency.

B. Analytical results

For a pure tone with angular frequency ω, the cilia displacement is given as

$$u(t,s) = u_m(\omega,s)\sin[\omega t + \Phi(\omega,s)], \qquad (6)$$
$$u_m = I_0 Am(\omega,s).$$

Here I_0 denotes stapes amplitude, $Am(\omega,s)$ is the product of the magnitude of the transfer functions for the basilar membrane and fluid–cilia coupling, and $\Phi(\omega,s)$ is the sum of their respective phases. In terms of the dimensionless cilia displacement $y = u/u_m$, scaled so that $-1 \leqslant y \leqslant 1$, the displacement-dependent conductance function in Eq. (5) takes the form

$$g(y) = \tilde{g}(u_m y) = e^{\alpha y}/(1+\beta e^{\alpha y}) - 1/(1+\beta), \qquad (7)$$

where $\alpha = u_m/(RT/Z_1)$; α is a dimensionless parameter measuring the degree of nonlinearity in $g(y)$.

Here we shall concentrate on asymptotic solutions of Eq. (5) for large and small α. We note that for large α, $g(y)$ is asymptotically an asymmetrical step function:

$$g(y) \equiv g_u = 1/[\beta(\beta+1)], \quad 0 < y \leqslant 1, \qquad (8)$$
$$g(y) \equiv g_l = -1/(1+\beta), \quad -1 \leqslant y < 0,$$

while for small α, $g(y)$ is a linear function with correction terms

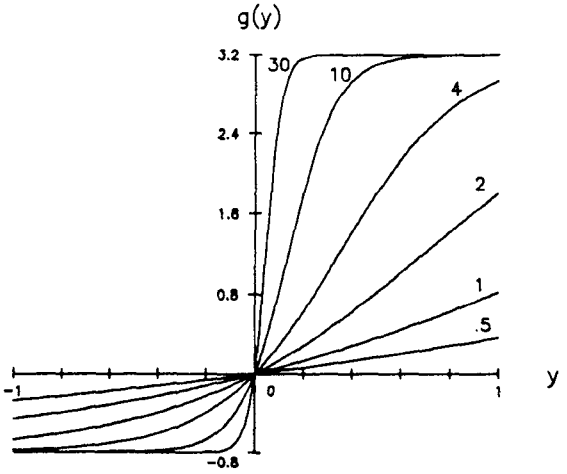

FIG. 9. Normalized hair cell conductance as a function of normalized cilia displacement. Equation (7) is plotted with $\beta = \frac{1}{4}$ and α as a parameter whose values label the different curves. The conductance is almost linear for $\alpha < 1$; for large values of α the conductance approaches an asymmetrical step function.

$$g(y) = [\alpha/(1+\beta)^2]y + [(1-\beta)\alpha^2/2(1+\beta)^3]y^2 + \cdots . \quad (9)$$

The function $g(y)$ is plotted in Fig. 9 to show the transition from linear to steplike behavior with increasing amplitude.

1. Hair cell dc response

For a pure tone, the dc response can be found by integration of Eq. (5) over a complete cycle. After a change of variable, $y = \sin(t)$, we obtain

$$v_{dc} = \pi^{-1}\int_{-1}^{1} \frac{g(y)}{\sqrt{(1-y^2)}\,dy} . \quad (10)$$

For large α, we use the step function approximation to $g(y)$ given by Eq. (8) to obtain

$$v_{dc} = (g_u + g_l)/2 + O(\alpha e^{-\alpha}). \quad (11)$$

Thus the dc response saturates to the mean value of the input (i.e., dimensionless conductance in this scaling and approximation) for large enough stapes amplitudes independent of frequency. For the parameter values used in Fig. 8(b), v_{dc} in dimensional form takes the value 3.87 mV, which differs only slightly from the asymptotes in Fig. 8(b); this difference is due primarily to approximating Eq. (3) by Eq. (5).

For small α, we use Eq. (9) to approximate the conductance in Eq. (10). By symmetry, the linear term does not contribute to the integral. This is expected since a linear conductance–displacement relation should not produce a dc response. The quadratic term does contribute, however:

$$v_{dc} = (\tfrac{1}{4})[(1-\beta)/(1+\beta)^3]\alpha^2 + O(\alpha^4). \quad (12)$$

This is an interesting result in that for small amplitudes, the dc response is proportional to the square of $Am(\omega,s)$, and hence sharper than the mechanical response. This effect can be seen when comparing Fig. 7(a) (note linear scale) with Fig. 7(c). Equation (12) also explains the parabolic behavior of the curves near the origin of Fig. 8(b) (see inset).

2. Hair cell ac response

The voltage waveform near saturation is obtained by integration of Eq. (5) using Eq. (8) to approximate the conductance. The result is expressed in terms of the exponentials:

$$v(\theta) = g_u + (v_0 - g_u)e^{-\theta/\omega\tau}, \quad 0 \leqslant \theta \leqslant \pi,$$
$$= g_l + D_0 e^{-(\theta-\pi)/\omega\tau}, \quad \pi \leqslant \theta \leqslant 2\pi, \quad (13)$$

where θ is the phase measured relative to the cilia displacement and $v_0 = v(0)$. The constant D_0 is formed by requiring continuity at $\theta = \pi$,

$$D_0 = (g_u - g_l) + (v_0 - g_u)e^{-\pi/\omega\tau} \quad (14)$$

and v_0 is found from the periodicity condition $v(0) = v(2\pi)$,

$$v_0 = g_u - (g_l - g_u)(1 - e^{-\pi/\omega\tau})/(1 - e^{-2\pi/\omega\tau}). \quad (15)$$

These relations predict the waveforms shown in Fig. 5(b). The peak-to-peak response is

$$v_{ac} = v(\pi) - v_0(1/\beta)(1 - e^{-\pi/\omega\tau})^2/(1 - e^{-2\pi/\omega\tau}). \quad (16)$$

At low frequencies $v_{ac} \sim 1/\beta = g_u - g_l$, while at high frequencies $v_{ac} \sim \pi/(2\beta\omega\tau)$. Thus the frequency response is that of a low-pass filter with a high-frequency slope of -6 dB/oct. This behavior is also shown in the computed frequency response for large amplitudes shown in Fig. 7(b). It is worth noting that more accurate representations of the waveform have been obtained for large α. In the neighborhood of $\theta = 0,\pi$ the approximation of Eq. (8) breaks down. Transition layer expressions constructed for these regions can be asymptotically matched to the given solution. These corrections smooth the sharp corners of the waveform at $\theta = 0,\pi$.

For small amplitudes, the voltage waveforms are nearly sinusoidal. Using Eq. (9) to approximate the conductance, the solution of Eq. (5) can be written as a sum of a dc component and oscillatory terms having frequencies ω, 2ω, 3ω,... . The magnitude of the fundamental is

$$\alpha[1 + (\omega\tau)^2]^{-1/2}/(1+\beta)^2 + O(\alpha^3). \quad (17)$$

For small amplitudes this closely approximates the peak-to-peak response, and explains the low amplitude behavior in Fig. 7(b) as essentially the product of the basilar membrane, fluid–cilia coupling, and linearized hair cell transfer functions. In Fig. 8(a) the large stapes amplitude behavior is adequately given by Eq. (16), while the linear behavior at small amplitudes is explained by Eq. (17).

IV. DISCUSSION

The model presented in this report is a minimal synthesis of the various stages of cochlear processing. It consists of three primary components: a linear basilar membrane, a linear fluid–cilia coupling stage, and an inner hair which incorporates a saturating nonlinearity due to the transduction process. The parameters of the model have reasonable physiological interpretations and their numerical values are derived when possible from published experimental measure-

ments. The mathematical treatment of the model results in relatively simple equations that allow an intuitive and analytical understanding of the numerically computed solutions. The present analysis of the model is restricted to frequencies below 1.5 kHz. We will first discuss the results of our model in light of comparable experimental data and then interpret them from the point of view of the tonotopic code and its intensity invariance.

The computed responses to single tone inputs fall in the physiologic range and display the major qualitative features of hair cell intracellular potentials and auditory nerve fiber activity such as frequency tuning (Fig. 7), rectified waveforms (Fig. 5) (Hudspeth and Corey, 1977), and saturating rate-level and synchrony-level functions (Fig. 8) (Kiang 1965, 1980; Rose *et al.*, 1967, 1971; Russell and Sellick, 1978; Sellick and Russell, 1980).

The computed results also account for two experimentally observed effects of the stimulus intensity of the frequency tuning of ac response measures. The first effect is the broadening of the response bandwidth with increasing sound intensity (Dallos and Santos-Sacchi, 1983), a trend which, in our model [Fig. 7(b)], is caused by the saturating nonlinearity. The second effect of increasing stimulus intensity is the downward shift of the BF of the hair cell recorded ac response (Dallos and Santos-Sacchi, 1983). This shift is present in the computed responses [Fig. 7(b)] and can be traced to the combined influences of the nonlinearity and of the low-pass action of hair cell capacitive membranes. While our calculated responses show qualitative agreement with the experimental data of Dallos and Santos-Sacchi (1983), the sharper second peak shown in their Fig. 2 is not reproduced in the present model, and often does not appear in their data (Dallos, 1984). We note that the bandwidth broadening and BF shifts have also been observed in the phase locked responses of auditory nerve fibers (BF$\geqslant$1000 Hz) in experiments using noise stimuli and reverse correlation methods to obtain the fibers' "transfer functions" (Evans, 1977; Harrison and Evans, 1982; Moller, 1978; Moller 1983a,b).

The model's dc isointensity curves also display a bandwidth increase with intensity. However, unlike the ac response, the peaks of the dc response curves do not shift downwards, but rather slightly upwards [Fig. 7(c)]. Similar behavior is observed in recorded isointensity responses of auditory nerve fibers using average rate measures of the activity (Kiang, 1980; Moller, 1983a).

It is difficult to compare directly our computed responses versus stapes amplitude functions [Fig. 8(a),(b)] with experimental data, since there is a lack of recordings of hair cell ac and dc potentials versus sound intensity in cochlear apical units with BF's below 1.5 kHz (the frequency range of our model). Our computed functions [Fig. 8(a),(b)] nevertheless resemble functions recorded in hair cells of the basal turn of the cochlea (responding to low-frequency tones) (Patuzzi and Sellick, 1983; Russell and Sellick, 1978; Sellick and Russell, 1979) and in auditory nerve fibers (Kiang, 1980). In particular, the saturating ac functions reproduce two experimentally observed features: (1) decreasing saturation levels with increasing frequency, which we attribute to the combined effect of the saturating nonlinearity followed by the hair cell low-pass filter and (2) horizontal positioning for different frequencies which reflects the frequency tuning of the cascade (i.e., for low intensity, the BF curve is leftmost). The computed dc functions also display such horizontal positioning, but a relatively weak saturation level dependence on frequency. This also agrees with experimental measurements (both at the hair cell and auditory nerve fiber levels) at frequenices below the BF of the unit (Sachs and Abbas, 1974; Evans, 1975; Patuzzi and Sellick, 1983).

The only nonlinearity considered in the present composite model is that of the hair cell transduction process. The asymmetry in the form of this nonlinearity is crucial to the generation of the dc responses and is responsible for their quadratic dependence on the stapes amplitude (in contrast to the linear dependence of the ac response) at low intensities (Fig. 8). This type of dependence, which has been predicted earlier in phenomenological models (Engebretson and Eldredge, 1968) and recently demonstrated experimentally (Patuzzi and Sellick, 1983), explains the sharper low-frequency slopes of the isointensity dc response curves [Fig. 7(c)] compared to those of the ac response curves [Fig. 7(b)].

There is at present a considerable variety of views about the nature and extent of nonlinearities in basilar membrane motion and fluid–cilia coupling mechanisms (Chadwick *et al.*, 1980; Evans, 1975; Holton and Weiss, 1983a,b; Kim and Molnar, 1975; Palmer and Evans, 1980; Patuzzi and Sellick, 1983; Rhode, 1971; Sellick *et al.*, 1983; Transcripts, 1980). We have elected to use a linear basilar membrane model since it affords a great deal of mathematical tractability and physiological relevance without sacrificing the major observed qualitative features of basilar membrane motion (Chadwick *et al.*, 1980). Nonlinear mechanisms for the generation of hair cell potentials and nerve spike trains, considered here and in other theoretical studies (Engebretson and Eldredge, 1968; Pfeiffer, 1970; Schroeder and Hall, 1974) have been shown capable of accounting for the various nonlinear phenomena such as two-tone suppression, saturation, and rectification. However, propagating combination tones (Kim *et al.*, 1980) and the possible active tuning (Kim, 1980; Siegel and Kim, 1982; Weiss, 1982) are two phenomena that could involve nonlinearities at the basilar membrane (or its coupling properties to the hair cells). Some descriptive models without explicit biophysical components have been proposed to account for these phenomena (de Boer, 1983; Neely and Kim, 1982). However, to explore adequately a variety of mechanisms in the context of our physiological approach is beyond the scope of this paper.

We finally discuss aspects of the experimental identification of a unit's BF, and the consequences of the intensity and stage-dependent BF shifts for this identification and more generally for the interpretation of a place or tonotopic code. In the traditional view of the place code there exists a one-to-one correspondence between the frequency of a pure tone and the spatial location of maximal mechanical and electrical response along the cochlear partition. By inverting this mapping we may associate with each location a frequen-

cy which is referred to here as the *global BF*. The experimental determination of the global BF is difficult (Pfeiffer and Kim, 1975) and so an alternate measurement has been widely made using swept tones. In this method the BF for a specific location is identified from the maximum of the isointensity response curve (which agrees at low intensities with the BF from the minimum of the threshold tuning curve). A BF determined using swept tones will be referred to here as a *local BF*. In general, the global and local BF's are not the same and both may be stage and intensity dependent. In our model, the local BF varies with stage and intensity whereas the global BF does not. The stage dependence of the local BF results from the combined effects of the high-pass filter in the fluid–cilia coupling stage and the low-pass action of the hair cell membranes. The intensity dependence results from the nonlinear conductance–displacement relation in the hair cell. In contrast, the global BF in our model does not depend on either stage or intensity. It is stage invariant because the mechanical and electrical parameters of the hair cells and fluid–cilia coupling are independent of s, and because its determination involves a single frequency; it is intensity invariant because the nonlinearity acts only after any s-dependent stages that may occur.[4] In theory and experiment one may find the consequences of such BF shifts. The isointensity ac response may sometimes bear little relationship to the global tuning of the basilar membrane. An extreme case in point here is the hair cells of the basal turn, which show larger ac responses for an 80 dB SPL tone at 6 kHz than at their nominal BF (e.g., 17 kHz) [Russell and Sellick, 1978, Fig. 3(d)]. On the other hand, a local BF determined from a hair cell dc response curve could be close to the corresponding global BF, particularly at low intensities and away fron the apical end where mechanical tuning is broad. All these discrepancies between the global BF and its local measurement become smaller for sharper basilar membrane tuning.

For a tonotopic code to provide information that is easily interpreted by the brain, it would seem desirable that a one-to-one correspondence between place (or auditory nerve fiber identity) and global BF be preserved under intensity changes. This is what we mean by tonotopic intensity invariance. In this sense the present model is tonotopically invariant, as would be any model based upon linear mechanics and a monotonic nonlinear hair cell electrodynamics which is s independent. A system with significant mechanical nonlinearity or significant spatial dependence in nonlinear properties in latter cochlear stages would likely not exhibit tonotopic invariance. In such cases, one has to conclude either that the tonotopic map of the auditory system is not used to derive the relatively invariant pitch percepts, or that complex central auditory mechanisms exist which would unravel the global BF shifts to deduce unambiguously the stimulus intensity and frequency characteristics.

The above considerations largely carry through to the case of complex sounds where, in addition, other effects have to be considered, such as the generation of distortion products, and synchrony and rate suppression (Young and Sachs, 1979).

APPENDIX: EQUATIONS FOR BASILAR MEMBRANE MOTION

Explicit relations are given here that describe the response (displacement w) of the basilar membrane model to a pure tone when the frequency is less than 1500 Hz. The relations given below are intended to provide interested readers with an explicit, self-contained computational recipe that is previously unpublished. The definitions of the variables and parameters are summarized in Table AI. The formulas incorporate spatially variable basilar membrane width, thickness, and cross-sectional chamber dimensions. The edges of the membrane are simply supported, and the shape of a chamber is a rectangle with width: height in the ratio 2:1.

$$w(s,x,T) = -(8/\pi)\rho^{1/2}B^{5/2}D_0^{-1/2}\Omega d_s \times A_r \cos[\pi x/2F(s)] \times \mathrm{Re}\left(\frac{P(s)\exp(i\Omega T)\sin(\epsilon^{-1}\int_1^s k(s')ds')}{f(s)\cos(\epsilon^{-1}\int_0^1 k(s')ds')}\right), \quad \text{(A1)}$$

$$k(s) = \alpha_0^{-1/2}k_0(s) + \alpha_0^{-3/2}k_1(s), \quad \text{(A2)}$$

$$k_0^2(s) = 16F(s)\{\pi^2 H^2(s)[1 - 3\delta(s)]f(s)\}^{-1}, \quad \text{(A3)}$$

TABLE AI. Definition of quantities used in basilar membrane model.

A	=	scaled chamber area (dimensionless)
A_r	=	ratio of oval window area to chamber area at basal end (dimensionless)
B	=	maximum basilar membrane half-width (cm), used to scale cross-plane dimensions
C_0	=	partition damping constant (dimensionless), $C'B^4/D_0$
C'	=	dimensional damping constant (dyn/cm^3)
d_s	=	stapes amplitude (cm)
D_0	=	maximum basilar membrane bending stiffness (dyn-cm)
D	=	scaled bending stiffness function (dimensionless)
F	=	scaled basilar membrane half-width (dimensionless)
h	=	scaled basilar membrane thickness (dimensionless)
h_0	=	maximum basilar membrane thickness (cm)
H	=	scaled chamber height (dimensionless)
i	=	$\sqrt{-1}$
k	=	scaled wavenumber (dimensionless)
L	=	length of basilar membrane (cm), used to scale longitudinal dimension
M_0	=	basilar membrane mass parameter (dimensionless), equal to $\mu B^4\Omega^2/D_0$
M	=	basilar membrane mass function (dimensionless)
P	=	scaled chamber perimeter (dimensionless)
s	=	longitudinal coordinate, scaled by L (dimensionless), see Fig. 2(a)
T	=	time (s)
w	=	basilar membrane displacement (cm)
x	=	transverse coordinate, scaled by B (dimensionless), see Fig. 2(a)
α_0	=	$D_0/(\rho B^5\Omega^2)$ frequency expansion parameter (dimensionless)
ϵ	=	B/L slenderness ratio
μ	=	characteristic mass/area (g/cm^2) of basilar membrane partition used in definition of M_0, equal to basilar membrane density times h_0
ν	=	kinematic viscosity (cm^2/s)
ρ	=	fluid density (g/cm^3)
Ω	=	angular frequency (rad/s)

TABLE AII. Correspondence in notation.

Present	(Chadwick, 1985)
$F(s)$	$G(x)$
s	x
x	y
α_0	α
C_0 (damping constant)	not used
not used	C_0 (constant pertaining to stapes amplitude)

$$\delta(s) = (i\Omega B^2/\nu)^{-1/2}/H(s), \tag{A4}$$

$$f(s) = D(s)\{\pi/[2F(s)]\}^4 - M_0 M(s) + i\Omega C_0, \tag{A5}$$

$$\frac{k_1(s)}{k_0(s)} = \frac{32F(s)[1 + (5/2)\delta(s)]}{[9\pi^2 f(s)]} + \frac{\delta(s)}{[3H(s)]} \sum_{m=1}^{\infty} \frac{(-1)^m B_m(s)}{\gamma_m(s)} - \frac{5\pi}{18} \sum_{m=1}^{\infty} B_m(s) K_m(s) \coth[\gamma_m(s) H(s)], \tag{A6}$$

$$\gamma_m(s) = m\pi/H(s); \quad m = 1,2,\ldots, \tag{A7}$$

$$K_m(s) = \frac{\pi}{2F^2(s)} \frac{\cos[\gamma_m(s)F(s)]}{[\pi/2F(s)]^2 - \gamma_m^2(s)} \quad \text{if } \gamma_m \neq \frac{\pi}{(2F)},$$

$$K_m(s) = \tfrac{1}{2} \quad \text{if } \gamma_m = \pi/(2F) \tag{A8}$$

$$B_m(s) = -\{16/[H(s)F(s)f(s)\gamma_m(s)]\}K_m(s), \tag{A9}$$

$$P(s) = (2k_0(s)H^2(s)\{1 - \alpha_0^{-2}[k_1(s)/k_0(s)]^2\})^{-1/2}. \tag{A10}$$

These formulas are based on a theory (Chadwick, 1985) that utilizes the WKB approximation applied to a three-dimensional model, and then uses further asymptotics in the cross plane to determine the wavenumber explicitly. Several notational changes had to be made here that should be noted when referring to (Chadwick, 1985). These are given in Table AII.

[1]References in this paper to the apical portion or apical membrane of the hair cell are meant to include the membrane of the cilia since the exact location of the mechanically sensitive channels is at present still uncertain.

[2]The parameter values shown in Table I are estimated to be within the physiologic range for a diverse set of experimental conditions and hence are not intended to duplicate accurately any particular preparation. The hair cell model presented in this report is quite robust in that the observed features of the computed responses do not critically depend on any one or set of parameter values. For the basilar membrane, care was taken to make sure that all parameters are consistent. For example, L, B, F, h_0, h, and H are all derived from Fernandez (1952) on the guinea pig, and D_0 was selected by fitting the model to low-frequency guinea pig data obtained by von Békésy (1960). However, lack of adequate experimental data necessitates the approximation of certain parameters, such as ρ. These were chosen to be within reasonable physiological ranges.

[3]Hereafter we shall refer to the frequency of peak response as the best frequency, BF. Note, however, that in general this definition depends on both stage and amplitude. Our presentation shall make this distinction explicit if the context does not clearly reveal it.

[4]These conclusions on global BF invariance can be understood as follows. For a fixed frequency, consider the input–output properties of the feedforward cascade. The amplitude of the hair cell response $\mathbf{H}$ is a nonlinear function of the cilia displacement which itself is represented as the product of intensity I_0 with the transfer functions $\mathbf{F}$ and $\mathbf{B}(s)$ of the fluid–cilia and basilar membrane stages, respectively: $\mathbf{H} = \mathbf{H}[I_0,\mathbf{F},\mathbf{B},(s)]$. Global BF derives from the value of s where $\mathbf{H}$ reaches a maximum, i.e., by the chain rule, s must satisfy $0 = \partial\mathbf{H}/\partial s = \mathbf{H}'\cdot I_0\cdot\partial\mathbf{B}/\partial s$, where $\mathbf{H}'$ is the derivative of $\mathbf{H}$ with respect to its argument. Note that, since the hair cells are identical, $\mathbf{H}$ does not depend explicitly on s. Thus when $\mathbf{H}$ is monotonic (i.e., $\mathbf{H}' \neq 0$), as in our case, the global BF is determined by $\mathbf{B}$ and is independent of I_0. Note that the I_0 independence would still hold even if cilia properties ($\mathbf{F}$) depend on s.

Allen, J. B. (1980). "A cochlear micromechanical model of transduction," Proceedings of the 5th International symposium on Hearing (Delft U. P., The Netherlands), pp. 85–95.

von Békésy, G. (1960). *Experiments in Hearing* (McGraw-Hill, New York).

de Boer, E. (1983). "Power amplification in an active model of the cochlea-short-wave case," J. Acoust. Soc. Am. 73, 577–579.

Boyce, W. E., and Diprima, R. C. (1977). *Elementary Differential Equations and Boundary Value Problems* (Wiley, New York), pp. 15–16.

Chadwick, R. S. (1985). "Three dimensional effects on low frequency cochlear mechanics," Mech. Res. Comm. 12, 181–186.

Chadwick, R. S., and Cole, J. D. (1979). "Modes and waves in the cochlea," Mech. Res. Comm. 6(3), 177–184.

Chadwick, R. S., Fourney, M. E., and Neiswander, P. (1980). "Modes and waves in a cochlear model," Hear. Res. 2, 475–483.

Corey, D. P., and Hudspeth, A. J. (1983a). "Analysis of the microphonic potential of the bullfrog's sacculus," J. Neurosci. 3 (5), 942–961.

Corey, D. P., and Hudspeth, A. J. (1983b). "Kinetics of the receptor current in bullfrog saccular haircell," J. Neurosci. 3 (5), 962–976.

Dallos, P. (1984). Personal communication.

Dallos, P. (1973). *The Auditory Periphery* (Academic, New York).

Dallos, P., and Santos-Sacchi, J. (1983). "AC receptor potentials from hair cells in the low-frequency region of the guinea pig cochlea," in *Mechanisms of Hearing*, edited by W. Webster and L. Aitkin (Monash U. P., Australia).

Dallos, P. (1983). "Some electrical circuit properties of the organ of Corti. I. Analysis without reactive elements," Hear. Res. 12, 89–119.

Davis, H. (1965). "A model for transducer action in the cochlea," Cold Spring Harbor Symp. Quant. Biol. 30, 181–190.

Engebretson, A. M., and Eldredge, D. (1968). "Model for nonlinear characteristics of cochlear potentials," J. Acoust. Soc. Am. 44, 548–554.

Evans, E. F. (1975). "Cochlear nerve and cochlear nucleus," in *Handbook of Sensory Physiology, Vol. 2* (Springer, Berlin), pp. 1–108.

Evans, E. F. (1977). "Frequency selectivity at high signal levels of single units in cochlear nerve and nucleus," in *Psychophysics and Physiology of Hearing*, edited by E. F. Evans and J. P. Wilson (Academic, New York), pp. 185–192.

Fernandez, C. (1952). "Dimensions of the cochlea (guinea pig)," J. Acoust. Soc. Am. 24, 519–523.

Flanagan, J. L. (1972). *Speech Analysis Synthesis and Perception* (Springer, Berlin).

Flock, A., and Strelioff, D. (1984). "Studies on haircells in isolated coils from the guinea pig cochlea," Hear. Res. 15, 11–18.

Harrison, R. V., and Evans, E. V. (1982). "Reverse correlation study of cochlear filtering in normal and pathalogical guinea pig ears," Hear. Res. 6, 303–314.

Holmes, M., and Cole, J. (1984). "Cochlear mechanics: Analysis for a pure tone," Dep. Math. Sci., Rensselaer Polytech. Inst., Troy, N. Y. (AD-A13643819).

Holton, T., and Weiss, T. F. (1983a). "Receptor potentials of lizard cochlear hair cells with free-standing stereocilia in response to tones," J. Physiol. 345, 205–240.

Holton, T., and Weiss, T. F. (1983b). "Frequency selectivity of hair cells and nerve fibers in the alligator lizard cochlea," J. Physiol. 345, 241–260.

Hudspeth, A. J., and Corey, D. P. (1977). "Sensitivity, polarity, and conductance change in the response of vertebrate hair cells to controlled mechanical stimuli," Proc. Nat. Acad. Sci. 74(6), 2407–2411.

Kiang, N. Y. (1965). "Discharge patterns of single fibers in the cat's auditory nerve," Res. Mono. No. 35 (MIT, Cambridge, MA).

Kiang, N. Y. (1980). "Processing of speech by the auditory nervous system," J. Acoust. Soc. Am. 68, 830–835.

Kim, D. O. (1980). "Cochlear mechanics: Implications of electrophysiolo-

gical and acoustical observations," Hear. Res. **2**, 297–317.
Kim, D. O., and Molnar, C. E. (**1975**). "Cochlear mechanics: Measurements and models," in *The Nervous System, Vol. 3*, edited by D. B. Tower (Raven, New York), pp. 57–68.
Kim, D. O., Molnar, C. E., and Matthews, J. W. (**1980**). "Cochlear mechanics: Nonlinear behavior in two-tone responses as reflected in cochlear-nerve-fiber responses and in ear-canal sound pressure," J. Acoust. Soc. Am. **67**, 1704–1721.
Lewis, R. S., and Hudspeth, A. J. (**1983**). "Voltage- and ion-dependent conductances in solitary vertebrate hair cells," Nature **304**, 538–541.
Moller, A. R. (**1978**). "Frequency selectivity of the peripheral auditory analyzer studied using broad band noise," Acta Physiol. Scand. **104**, 24–32.
Moller, A. R. (**1983a**). "Frequency selectivity of phase-locking of complex sounds in the auditory nerve of the rat," Hear. Res. **11**, 267–284.
Moller, A. R. (**1983b**). "Use of pseudorandom noise in studies of frequency selectivity: the periphery of the auditory system," Biol. Cybern. **47**(2), 95–102.
Morrish, K. A., Chadwick, R. S., Shamma, S. A., and Rinzel, J. (**1986**). "Parameter sensitivity in a mathematical model of basilar membrane mechanics," in *Peripheral Auditory Mechanisms*, edited by J. B. Allen, J. L. Hall, A. Hubbard, S. T. Neely, and A. Tubis (Springer, New York).
Neely, S. T., and Kim, D. O. (**1982**). "An active cochlear model shows sharp tuning and high sensitivity," Hear. Res. **9**, 123–130.
Palmer, A. R., and Evans, E. F. (**1980**). "Cochlear fiber rate-intensity functions: no evidence for basilar membrane nonlinearities," Hear. Res. **2**, 319–326.
Patuzzi, R., and Sellick, P. M. (**1983**). "Basilar membrane motion and inner hair cell output," J. Acoust. Soc. Am. **74**, 1734–1741.
Pfeiffer, R. (**1970**). "A model for two-tone inhibition of single cochlear-nerve fibers," J. Acoust. Soc. Am. **48**, 1373–1378.
Pfeiffer, R., and Kim, D. (**1975**). "Cochlear nerve fiber responses: Distribution along the cochlear partition," J. Acoust. Soc. Am. **58**, 867–869.
Rhode, W. S. (**1971**). "Observations of the basilar membrane in squirrel monkey using the Mossbauer technique," J. Acoust. Soc. Am. **49**, 1218–1231.
Rose, J. E., Brugge, J. F., Anderson, D. J., and Hind, J. E. (**1967**). "Phase-locked responses to low frequency tones in single auditory nerve fibers of the squirrel monkey," J Neurophysiol. **30**, 769–792.
Rose, J. E., Hind, J. E., Anderson, D. J., and Brugge, J. F. (**1971**). "Some effects of stimulus intensity on response of auditory nerve fibers in the squirrel monkey," J. Neurophysiol. **34**, 685–699.
Russell, I. J., and Sellick, P. M. (**1978**). "Intracellular studies of hair cells in the mammalian cochlea," J. Physiol. (London) **284**, 261–290.
Russell, I. J. (**1983**). "Origin of the receptor potential in inner hair cells of the mammalian cochlea—evidence for Davis' theory," Nature **301** (27), 334–336.
Sachs, M., and Abbas, P. (**1974**). "Rate versus level functions for auditory-nerve fibers in cats: Tone-bursts stimuli," J. Acoust. Soc. Am. **56**, 1835–1847.
Schroeder, M., and Hall, J. (**1974**). "A model for mechanical to neural transduction in the auditory receptor," J. Acoust. Soc. Am. **55**, 1055–1060.
Sellick, P. M., and Russell, I. J. (**1979**). "Two-tone suppression in cochlear hair cells," Hear. Res. **1**, 227–236.
Sellick, P. M., and Russell, I. J. (**1980**). "The responses of inner hair cells to basilar membrane velocity during low frequency auditory stimulation in the guinea pig cochlea," Hear. Res. **2**, 439–445.
Sellick, P. M., Patuzzi, R., and Johnstone, B. (**1982**). "Modulation of responses of spiral ganglion cells in the guinea pig cochlea by low frequency sound," Hear. Res. **7**, 199–221.
Sellick, P. M., Patuzzi, R., and Johnstone, B. (**1983**). "Comparison between the tuning properties of inner hair cells and basilar membrane motion," Hear. Res. **10**, 93–100.
Siegel, J. H., and Kim, D. O. (**1982**). "Efferent neural control of cochlear mechanics? Olivocochlear bundle stimulation affects cochlear biomechanical nonlinearity," Hear. Res. **6**, 171–182.
Smoorenburg, G. E., and Linschoten, D. H. (**1978**). "A neurophysiological study on auditory frequency analysis of complex tones," in *Psychophysics and Physiology of Hearing*, edited by E. Evans (Academic, London).
Terhardt, E. (**1975**). "Influence of intensity on the pitch of complex tones," Acoustica **33**, 5.
Transcripts of the mid-Symposium Discussion Period (**1980**). Hear. Res. **2**, 581–587.
Weiss, T. F. (**1982**). "Bidirectional transduction in vertebrate hair cells: A mechanism for coupling mechanical and electrical processes," Hear. Res. **7**, 353–360.
Weiss, T. F. (**1984**). "Relation of receptor potentials of cochlear hair cells to spike discharge of cochlear neurons," Ann. Rev. Physiol. **46**, 247–259.
Wever, E. G. (**1949**). *Theory of Hearing* (Dover, New York), pp. 340–346.
Wilson, J. P., and Evans, E. F. (**1983**). "Some observations on the 'passive' mechanics of cat basilar membrane," in *Mechanisms of Hearing*, edited by W. Webster and L. Aitkin (Monash U. P., Australia).
Young, E. D., and Sachs, M. B. (**1979**). "Representation of steady-state vowels in the temporal aspects of the discharge patterns of populations of auditory nerve fibers," J. Acoust. Soc. Am. **60**, 1381–1403.

A biophysical model of cochlear processing: Intensity dependence of pure tone responses

Shihab A. Shamma,[a] Richard S. Chadwick,[b] W. John Wilbur, Kathleen A. Morrish, and John Rinzel

Mathematical Research Branch, National Institute of Arthritis, Diabetes, Digestive and Kidney Diseases, National Institutes of Health, Bethesda, Maryland 20892

(Received 17 September 1984; accepted for publication 11 February 1986)

A mathematical model of cochlear processing is developed to account for the nonlinear dependence of frequency selectivity on intensity in inner hair cell and auditory nerve fiber responses. The model describes the transformation from acoustic stimulus to intracellular hair cell potentials in the cochlea. It incorporates a linear formulation of basilar membrane mechanics and subtectorial fluid–cilia displacement coupling, and a simplified description of the inner hair cell nonlinear transduction process. The analysis at this stage is restricted to low-frequency single tones. The computed responses to single tone inputs exhibit the experimentally observed nonlinear effects of increasing intensity such as the increase in the bandwidth of frequency selectivity and the downward shift of the best frequency. In the model, the first effect is primarily due to the saturating effect of the hair cell nonlinearity. The second results from the combined effects of both the nonlinearity and of the inner hair cell low-pass transfer function. In contrast to these shifts along the frequency axis, the model does not exhibit intensity dependent shifts of the spatial location along the cochlea of the peak response for a given single tone. The observed shifts therefore do not contradict an intensity invariant tonotopic code.

PACS numbers: 43.63.Bq

INTRODUCTION

Nonlinearities in cochlear function have been the focus of extensive experimental and theoretical study. One such phenomenon concerns the nonlinear dependence of the frequency selectivity of phase locking on stimulus intensity in the auditory nerve to simple and complex sounds (Moller, 1983a; Evans, 1977; Smoorenburg and Linschoten, 1978). With increasing intensity, the selectivity of the response transfer function deteriorates and the frequency of best response shifts downwards. Recent intracellular recordings of ac transfer functions of inner hair cells in the apical cochlear region exhibit similar dependence on stimulus intensity (Dallos and Santos-Sacchi, 1983). Moller (1978) attributed these effects to nonlinear broadening and downward shift of basilar membrane tuning. Other investigators (Evans, 1977; Wilson and Evans, 1983), however, demonstrated linear tuning of the basilar membrane at these intensity levels, and concluded that the deterioration may be due to effects in the hypothetical "second filter" between the membrane and the hair cells. Despite these downward shifts of the best frequency, psychophysical experiments show relatively slight dependence of pitch perception on intensity for single tones (Wever, 1949; Moller, 1978) and none at all for complex tones (Terhardt, 1975). These apparent contradictions would raise serious doubts regarding the intensity invariance of the cochlear tonotopic map and its relevance for pitch coding in the auditory system. In this report, we address this issue and demonstrate that a specific theoretical model using linear basilar membrane mechanics and space-independent fluid–cilia coupling can account for these intensity effects and yet maintain an intensity invariant tonotopic map.

A major part of our effort here involves developing a composite model of the various cochlear stages that is efficient to compute and is founded on basic principles and experimental data from the different constituents of the peripheral auditory system. We use the model to demonstrate the contribution of the various stages to the nonlinear intensity-dependent changes of the frequency tuning curves and other input/output measures of the response to single low-frequency tones.

A schematic of the basic building blocks of the model and their amplitude transfer characteristics is shown in Fig. 1. It is worth reiterating that these transfer characteristics are based on computations using mostly explicit biophysical parameters discussed in later sections and are not assumed *a priori*. The first stage is a linear, three-dimensional model of basilar membrane mechanics which incorporates basic physiological parameters in its formulation (Chadwick and Cole, 1979; Chadwick *et al.*, 1980). The present treatment is primarily valid for the low-frequency range (< 1500 Hz). At a given location along the cochlea the mechanical transfer function describes the ratio of basilar membrane displacement to stapes displacement as a function of stimulus frequency (i.e., the frequency tuning curve at that location). The basilar membrane displacement then produces an inner hair cell cilia displacement via the second block, which includes coupling of the cilia to the fluid in the subtectorial space. This stage exhibits the experimentally observed high-

[a] Present address: Electrical Engineering Department, University of Maryland, College Park, MD 20742.

[b] Present address: Biomedical Engineering and Instrumentation Branch, Division of Research Services, National Institutes of Health, Bethesda, MD 20892.

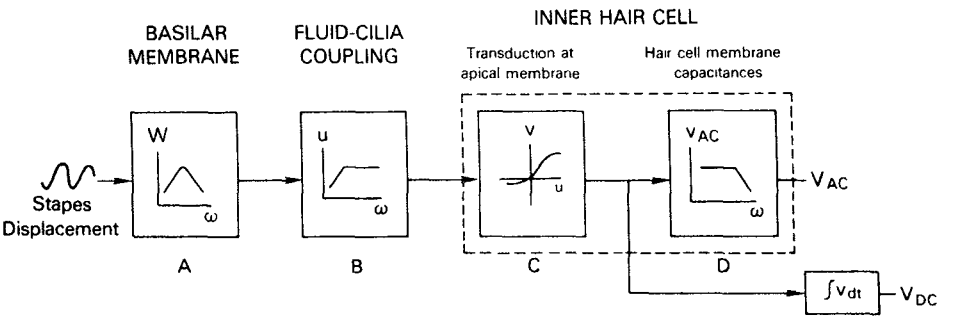

FIG. 1. Simplified block diagram of the processing stages of the composite cochlear model.

pass ("velocity") transfer function and assumes space-independent parameters (i.e., identical hair cell characteristics and cilia lengths). Our model for inner hair cell electrical activity is based on a simplified description of the anatomy and electrophysiology of the organ of Corti and on experimental studies of the nonlinear mechanisms of the hair cell ciliary transduction (Corey and Hudspeth, 1983a; Dallos, 1983; Russell and Sellick, 1978; Russell, 1983). Under certain assumptions its transfer characteristics can be subdivided into two elements: (1) The saturating, asymmetric, nonlinear transduction of cilia displacement into conductance changes of the apical membrane, which results in modulations of hair cell currents and of the intracellular potentials and (2) the capacitive effects of the hair cell membrane which attenuate the ac potentials at high frequencies. The final outputs computed from the model are the peak-to-peak value of the inner hair cell potential (an ac measure) and its average value (a dc measure). These measures are discussed with reference to experimentally recorded hair cell potentials as functions of frequency and intensity.

In Secs. I and II we develop the various stages of the model and discuss in detail the limitations of the assumptions and approximations that allow a simple and intuitive formulation to emerge. In Sec. III we present the computed responses of the model as functions of the frequency and intensity of a single tone. Finally, these results are analyzed in Sec. IV in light of the published data and certain conclusions regarding cochlear processing and neural encoding of sound are discussed.

I. COCHLEAR MECHANICS AND FLUID–CILIA COUPLING

A. Basilar membrane motion

The basilar membrane model has been discussed elsewhere (Chadwick and Cole, 1979; Chadwick *et al.*, 1980; Chadwick, 1985). The intent here is to summarize the essential ideas and approximations used in the model. The equations used to calculate the basilar membrane motion are given in the Appendix. The system consists of a slender, coiled, rigid tube having a variable cross-sectional area that is filled with a viscous, incompressible fluid. The tube is divided lengthwise into two chambers (scala vestibuli, scala tympani) by an interior surface, part of which is rigid and part viscoelastic (basilar membrane). The viscoelastic portion is a highly anisotropic plate having variable width and thickness, and a damping per unit area proportional to basilar membrane velocity. The system is driven by a prescribed pure tone stapes displacement at the basal end of the tube. At the apical end, pressure is equalized at the helicotrema. The plate deflects due to the pressure difference across it in the fluid, and the fluid motion is coupled locally to the plate motion. A sketch of the uncoiled model is shown in Fig. 2(a). The theory applies to the actual coiled geometry, however. All geometrical parameters in the model are chosen consistent with anatomical data for the guinea pig (Fernandez, 1952).

Amplitudes are assumed to be small enough that linearization of the hydrodynamics and elasticity should be a good approximation. In the present formulation the antisymmetric saturating nonlinearity of the hair cell conductance is taken to be the dominant nonlinearity (cf. Sec. IV). Furthermore, our solution methods here apply to the low-frequency end (< 1500 Hz) of the auditory range, where specialized asymptotics simplify the calculations. The resulting theory involves the three-dimensional motion of the fluid and can be shown to be a low-frequency limit of Holmes and Cole, 1984.

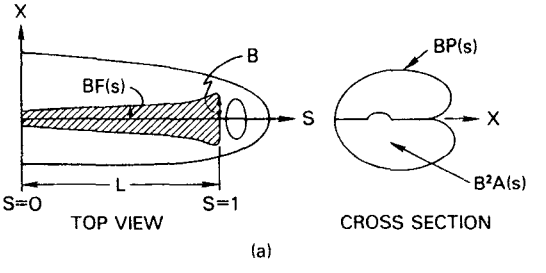

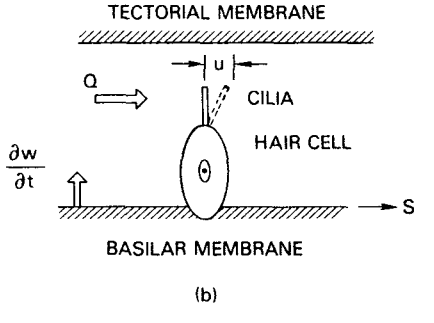

FIG. 2. (a) Top view and cross section of the basilar membrane model (see text, Appendix, and Table I for function definitions). (b) Schematic of fluid–cilia coupling stage. w = basilar membrane displacment, Q = fluid velocity, u = cilia displacement.

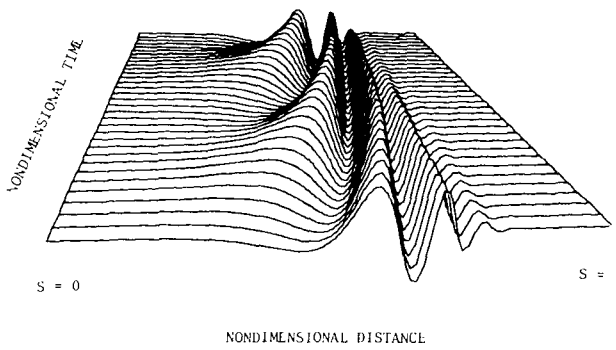

FIG. 3. Traveling wave displacement of basilar membrane model as a function of time and distance along the cochlea. Two periods are shown. The stimulus is a pure tone at 700 Hz; the parameters are those of Table I.

The nature of the computed basilar membrane waveform is shown in Fig. 3, where a perspective view of the center line plate deflection ($x = 0$) is plotted as a function of spatial location (s increasing from left to right) and time (increasing away from observer). Several features of the traveling wave are notable: The wavelength decreases, the phase velocity decreases, and the amplitude increases as the region of maximal response is approached. Both forward and reflected waves are included in the solution [cf. Eq. (A1)], but in this particular example at 700 Hz the reflected wave contribution to the response is negligible. At lower frequencies the reflected wave amplitude becomes larger. [A tuning curve for $s = 0.65$ is shown in Fig. 7(a).] The frequency of best response, 615 Hz, and the high-frequency slope, 31 dB/oct, both obtained at $s = 0.65$, are consistent with low-frequency experimental data (von Békésy, 1960) for the guinea pig. Note that the high-frequency slope is computed by performing a linear regression on all computed points between 6 and 12 dB below peak (Morrish *et al.*, 1986).

B. Fluid–cilia coupling

In contrast to outer hair cells, which are thought to be driven directly by the displacement of the basilar membrane, inner hair cells are not imbedded in the tectorial membrane, and so they instead must be driven by fluid motion. There is anatomical and electrophysical support for this hypothesis. For instance, tuning curves for intracellular recordings from inner hair cells exhibit low-frequency slopes that are 6 dB/oct steeper than those obtained from the outer hair cells (Dallos and Santos-Sacchi, 1983). To account for this effect, the following simple model is proposed [see Fig. 2(b)]. Let u be some measure of displacement of the inner hair cell cilia, e.g., linear displacement of the bundle tip or angular displacement at the root; u is the mechanical input to the hair cell model. We seek to find a relationship between u and basilar membrane displacement w. For the present discussion we can ignore the details of the velocity field distorting the cilia bundle, and simply refer to some spatial mean of the transverse component Q. Because of linearity, Q will be proportional to $\partial w/\partial t$, and the constant of proportionality depends on the geometry of the space between the apical surface of the hair cells and the tectorial membrane. Since the subtectorial gap is small, the Reynolds' number is small, and therefore the force deflecting the bundle will be proportional to the fluid velocity Q. The constant of proportionality depends on the geometry of the bundle and the viscosity of the endolymph. Resisting this deflecting force are an elastic force proportional to u and a dissipative force proportional to $\partial u/\partial t$. Since the individual cilia apparently behave like rigid rods and do not bend (Flock and Strelioff, 1984), the elastic force is due to an effective torsional spring at the base of the cilia bundle, and the dissipation is caused by the material holding together the bundle and perhaps internal dissipation in the individual cilia. These arguments then lead to the relation connecting w and u:

$$\tau_c \frac{\partial u}{\partial t} + u = \tau_c C \frac{\partial w}{\partial t}. \tag{1}$$

For simple harmonic motion this gives the transfer function

$$u/w = Ci\Omega\tau_c/(1 + i\Omega\tau_c). \tag{2}$$

The two constants in Eq. (2), the gain C and time constant τ_c, depend on the abovementioned proportionality relations. A sketch of the magnitude of the transfer function [Fig. 1(b)] shows its high-pass characteristics. The hair cell here is driven by velocity up to frequency ($1/2\pi\tau_c$) and by displacement beyond that. This pole primarily accounts for the apparent disappearance at higher frequencies (> 500–900 Hz) of a 90° phase lead between the inner and outer hair cell potentials (Dallos and Santos-Sacchi, 1983; Sellick and Russell, 1980; Sellick *et al.*, 1982). Alternative formulations have been advanced to deal with this issue (Dallos and Santos-Sacchi, 1983), but definitive experimental evidence is lacking at present (Sellick *et al.*, 1982). It should be noted, however, that the qualitative features of the computed magnitude transfer functions are relatively intensitive to τ_c. The transfer function of Eq. (2) has a gain $C(= 0.1)$ such that stapes displacements and corresponding cilia displacements and transduced hair cell potentials are all within physiologic ranges. Finally, note that this coupling is independent of position along the cochlea and hence is unlike the hypothetical "second filter" proposed by several investigators (e.g., Allen, 1980). A possible generalization of our present mode is to include an s-dependent cilia length which is observed in some species (Weiss, 1984), which would affect the time constant τ_c. In this case, τ_c is proportional to cilia length (l) since the viscous force varies directly with l, while the elastic restoring force (which is lumped at the cilia base) is independent of l.

II. INNER HAIR CELL DISPLACEMENT–VOLTAGE TRANSDUCTION

A. Hair cell model

In this section we develop and analyze a hair cell model based on experimental measurements of intracellular recordings in the hair cell of the guinea pig [(Dallos and Santos-Sacchi, 1983; Russell and Sellick, 1978) *in vivo*] and of the bullfrog sacculus [(Corey and Hudspeth, 1983a) *in vitro*]. We first derive a mathematical description of this model, then discuss assumptions and parameter considerations, and finally exploit several approximations that allow a simple and accurate description of the hair cell transfer charac-

teristics in both the linear and nonlinear regimes.

Our starting point is a somewhat simplified version of hair cell–epithelium equivalent circuit proposed by Cory and Hudspeth (1983a) (Fig. 4). It is in essence similar to the circuit of the "resistance microphonic" theory proposed in Davis (1965). In our circuit, only those components affecting the behavior of the intracellular potential responses are preserved. By applying Kirchoff 's current law to the equivalent circuit of Fig. 4, we derive an equation relating the intracellular hair cell potential V to the cilia displacement u:

$$(C_a + C_b)\frac{dV}{dt} + G(u)(V - E_t) + G_K(V - E'_K) = 0. \tag{3}$$

Here E_t is the endocochlear potential (Dallos, 1973) and $E'_K \approx E_K + E_t R_p/(R_t + R_p)$, where E_K is the reversal potential for ionic current [primarily dominated by K^+ (Lewis and Hudspeth, 1983; Corey and Hudspeth, 1983a)] across the basal membrane of the hair cell, here slightly corrected to E'_K to account for the extracellular pathway (shown dashed in Fig. 4) which sets up a nonzero extracellular resting potential near the basal membrane of the hair cell.

The resistance of the pathway through the hair cell membrane from the endolymph of the scala media to the perilymph of the scala tympani is much larger than that through the leaky epithelium, i.e., $1/R_t \gg G, G_k$ (Corey and Hudspeth, 1983a). (Similarly, the hair cell membrane capacitances greatly exceed the epithelial capacitance; therefore, the latter are not shown in Fig. 4.) As a consequence the extracellular potential remains essentially constant and we treat it as such in our model. The hair cell is thus decoupled from the epithelial circuit and neighboring hair cells. Perturbations of intracellular potential and of the trans-baso-lateral membrane potential become equivalent. These observations are consistent with experimental findings (Dallos, 1983). Furthermore, we assume that all the hair cell intracellular fluid space is equipotential and thus can be represented by a single node (Dallos, 1983).

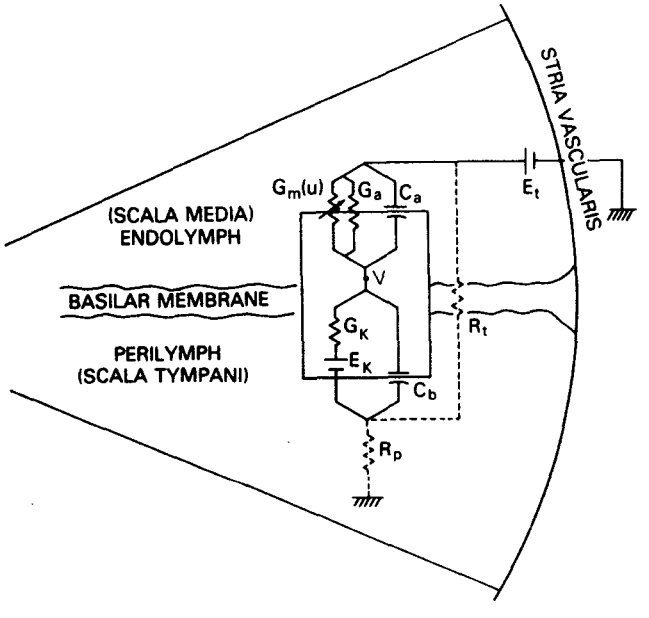

FIG. 4. Schematic diagram of a radial section of the cochlea, including the equivalent circuit of the inner hair cell and surrounding structures. E_t = endocochlear potential; R_t, R_p = epithelium resistances; E_K = potassium reversal potential; G_K = ionic channel conductance of the hair cell basal membrane; $G_m(u)$ = mechanically sensitive conductance of the hair cell apical membrane; G_a = leakage conductance of the hair cell apical membrane; u = cilia displacement; V = hair cell intracellular potential.

In this circuit we have retained only the primary contributions to membrane conductance: a conductance $G(u)$ in the apical portion[1] of the hair cell which includes a mechanically sensitive non-ion-selective transducer channel, and a K^+-dominated conductance (G_K) in the basal membrane. While several voltage-dependent ionic channels (K^+, Ca^{++}) are at present being investigated in vertebrate hair cells (Lewis and Hudspeth, 1983; Corey and Hudspeth, 1983b) (time constants 0.4–80 ms), relatively little information is available about such channels in mammalian hair cells. For this reason, and to keep our model simple, we here assume that G_K and $G(u)$ are not voltage dependent: G_K remains at its steady-state value (1.07×10^{-8} S). This value and the resting apical membrane resistance G_0 [$= G(0)$] are chosen to give a total steady-state hair cell resistance [$1/(G_0 + G_K)$] of 66 MΩ (Russell and Sellick, 1978) and a rest potential of approximately -28.4 mV (Russell and Sellick, 1978; Dallos and Santos-Sacchi, 1983).

The conductance of the apical membrane is the sum of a mechanically sensitive term $G_m(u)$ and a constant (leakage) term (Hudspeth and Corey, 1977; Russell and Sellick, 1978; Dallos, 1983). For the mechanically varying part we employ the direct coupling model proposed by Corey and Hudspeth (1983a) in their analysis of the bullfrog saccular hair cell. In this view, cilia displacement activates ionic channels directly rather than via chemical mediators. Experimental evidence suggests that the time constants (order of μs) for activation–inactivation processes are much shorter than the time scales of frequencies (< 1500 Hz) considered here (Corey and Hudspeth, 1983b). This allows the use of the Boltzmann distribution to represent the distribution of channel states as an instantaneous function of u. We may write the total mechanically sensitive conductance as the product of G_{max}, the conductance with all channels fully open, and $P_c(u)$, the fraction of channels in the open state. We determine P_c according to the Boltzmann distribution and assume a channel model with two states (open and closed) so that

$$G_m(u) = G_{max} P_c(u) = G_{max}/[1 + \exp(\Delta G_{act}/RT)], \tag{4}$$

where ΔG_{act} is the channel activation energy. Here ΔG_{act} is modeled simply as a linear function of displacement $\Delta G_{act} = G_1 - Z_1 u$. Note that G_m is partially activated at zero displacement but inactivates completely for large negative displacement. As Hudspeth and Corey (1977) point out, this description of conductance is analogous to that for an instantaneous voltage-activated channel in excitable nerve membrane. These authors also describe and utilize a three-state model which allows a more precise fit of their data, but for our purposes the qualitative features are adequately provided by the two-state theory. The values of G_1 and Z_1 that we use in our model are close to those used by Corey and

Hudspeth (1983a); G_{max} is chosen so that the total change in apical membrane resistance under maximum displacement is approximately 25% (Hudspeth and Corey, 1977; Dallos, 1983).

All the numerical results discussed in Sec. III are generated using Eq. (3). However, a further simplification of this equation allows easy and intuitive understanding of these results. By rewriting $G(u) = G_0 + \tilde{G}(u)$, we define $\tilde{G}(u)$ as the modulation of the conductance due to the cilia displacement. Similarly, we write $V = V_0 + \tilde{V}$, where V_0 is the intracellular resting potential and $\tilde{V}$ is the potential deviation from rest. For parameter values under consideration here we find that $\tilde{G}$ is sufficiently small relative to the total resting conductance $G_0 + G_K$ so that $\tilde{V}$ is small compared to $E_t - V_0$, the driving potential (relative to rest) for the displacement-activated conductance. Hence we can make the approximation $E_t - V \approx E_t - V_0$. Then by introducing dimensionless variables, Eq. (3) reduces to:

$$\tau \frac{dv}{dt} v = \tilde{g}(u), \tag{5}$$

where $\tau = (C_a + C_b)/(G_0 + G_k)$, $v = \tilde{V}(G_0 + G_k)/[\beta G_{max}(E_t - V_0)]$, $\tilde{g} = \tilde{G}/\beta G_{max}$, $V_0 = (G_0 E_t + G_k E_k')/(G_0 + G_k)$, and $\beta = \exp(-G_1/RT)$.

The hair cell then appears as a first-order low-pass filter with time constant τ. The "driving" term $\tilde{g}(u)$ is the result of nonlinear transduction from cilia displacement $u(t)$ to ionic conductance. The "output" potential v is the result of low-pass filtering the driving waveform. (See Fig. 1.)

B. Hair cell transfer characteristics

Figure 5(a) shows the intracellular potential V in response to a sinusoidal input function $u(t) = u_0 \sin(\omega t)$, applied at various amplitudes u_0. At the lowest amplitudes, the intracellular potential is sinusoidal and is linearly related to $u(t)$. At higher amplitudes, however, the effect of the saturating transducer nonlinearity becomes progressively larger. The troughs of the voltage waveforms saturate first [because of the asymmetry in $\tilde{g}(u)$], followed at higher amplitudes by the crests. In Fig. 5(b) the hair cell potential for a fixed amplitude u_0 is plotted over one period of the response for three different frequencies. The changes in the waveform with increasing frequency are due to the attenuation of the ac components by the hair cell membrane capacitances.

There are two distinct types of experimental measures of these waveforms that have been widely used. One is an *average* measure, which is the average value of the potential (deviation from rest) over one period. This measure increases for higher input amplitudes because of the increasing asymmetry in the waveform. It is therefore a direct consequence of the asymmetry in the transducer nonlinearity. Because this average evaluates the time-independent Fourier component in the waveform, we call it the dc measure. The second type of measure takes into account the *temporal* changes in the waveform over a period. One such measure is the peak-to-peak value; another is the amplitude of the first Fourier harmonic. Note that the deformed output waveform is not a pure sinusoid and hence contains several harmonics of the input frequency. We shall use the peak-to-peak value of the

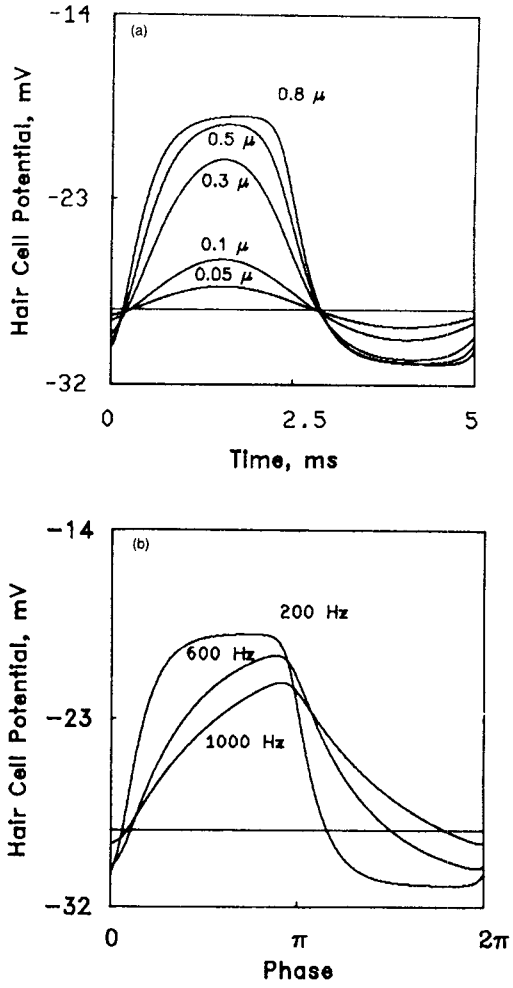

FIG. 5. (a) Waveform of hair cell intracellular potential in response to sinusoidal cilia displacement function $u(t) = u_0 \sin \omega_0 t$, where $\omega_0/2\pi = 200$ Hz and cilia displacement u_0 is the parameter. (b) Waveform of hair cell intracellular potential plotted versus phase over one period in response to sinusoidal displacement function $u(t) = u_0 \sin \omega t$, where cilia displacement $u_0 = 1$ μm, and frequency $\omega/2\pi$ is the parameter.

waveform as the ac measure. This measure is relatively easy to obtain experimentally and numerically, but is theoretically a complicated measure of all the harmonics.

1. Frequency responses—ac measures

Many investigators describe the transfer characteristics of a hair cell by its response as a function of the frequency of a constant amplitude sinusoidal input, i.e., by a "transfer function" (Corey and Hudspeth, 1983a; Dallos and Santos-Sacchi, 1983). This is convenient for the *in vivo* experiments where single tone stimuli are used. Also, such data are most easily interpretable for the linear regime of low tone intensity. However, for our theoretical model of Eq. (3) there are no simple correspondences between the input and output frequencies because the output $v(t)$ depends nonlinearly upon the input $u(t)$. It is, however, possible to predict the qualitative behavior of output ac measures based on the simplification of Eq. (5). For example, consider a sinusoidal cilia displacement $u(t) = u_0 \sin(\omega_0 t)$ of constant amplitude

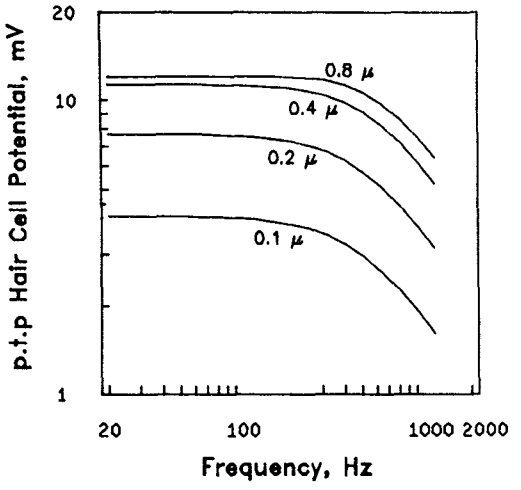

FIG. 6. Hair cell ac transfer characteristics. Each curve represents the peak-to-peak intracellular potential versus frequency of sinusoidal displacement presented at a certain maximum cilia displacement level (indicated by the associated parameter).

u_0. The nonlinearity $\tilde{g}(u)$ deforms $u(t)$ and results in a waveform composed of a dc term and several harmonics (the largest of which is the first harmonic). The output of the system v is then the superposition of these components, each acted upon separately by the same linear low-pass filter. Therefore, in sweeping the input frequency, *any ac measure of the output* will display a low-pass function of frequency. This is illustrated in Fig. 6, where each curve represents the peak-to-peak value of the potential [computed from Eq. (3)] plotted versus the frequency of a constant amplitude sinusoid. The effect of the saturating nonlinearity $\tilde{g}(u)$ is manifested in the "bunching up" of the curves at larger u_0 (output curves for $u_0 > 0.7$ μ cannot be easily distinguished).

2. Frequency responses—dc measures

Unlike the ac components, the dc measure is independent of the input frequency. This is precisely true for Eq. (5) and a good approximation for Eq. (3). At high frequencies ($\gg \frac{1}{2}\pi\tau$) the dc measure is the only surviving part in the response because the ac components attenuate drastically.

III. RESPONSE OF THE COMPOSITE MODEL TO SINGLE TONE STIMULI

Representative calculations will now be presented that show how a pure tone introduced at the stapes is transformed into intracellular potentials of inner hair cells. For fixed geometrical, mechanical, and electrical parameters in the model (see Table I),[2] the hair cell response depends on the frequency of the tone, the stapes amplitude, and the distance of the hair cell from the stapes. In this section we fix the distance at $s = 0.65$; the effects of location will be discussed in Sec. IV. We characterize the cochlear transformation in two ways. First, we determine the frequency dependence of the response with stapes amplitude as a parameter; Fig. 7(b) and (c) shows such isointensity plots of the inner hair cell potential for both ac and dc measures. Second, we compute

TABLE I. Parameter values.

$L = 1.85$ cm
$B = 0.0125$ cm
$\nu = 0.008$ cm^2/s
$D_0 = 0.094$ dyn/cm
$\rho = 1$ g/cm^3
$A(s) = 2h^2$
$F(s) = (8 + 5s)/13$
$P(s) = 6h$
$D(s) = h^3$
$h_0 = 0.0007$ cm
$h = 1 \quad s < 0.2$
$0.1 + 0.9\exp(0.7\text{–}3.5s), \quad s > 0.2$
$H = 6.5 - 17s, \quad s < 0.176$
$= 3.8 - 1.7s, \quad s > 0.176$
$C' = 115$ dyn/cm^3
$M = 3$
$C = 0.1$
$\tau_c = 0.3$ ms
$E_t = 100$ mV
$E_k = -84$ mV
$R_p/(R_p + R_t) = 0.04$
$C_a + C_b =$ pF
$G_k = 1.07\times10^{-8}$ S
$G_{max} = 0.15\times10^{-8}$ S
$G_0 = 0.43\times10^{-8}$ S
$Z_1/RT = 10\,\mu\text{m}^{-1}$
$\exp(-G_1/RT) = 0.25$

the ac and dc hair cell potential versus stapes amplitude with frequency as a parameter; Fig. 8(a) and (b) illustrates these functions. We will first discuss these numerical results (Figs. 7 and 8) in terms of the processing of a cascade of filters, with reference to the functional diagram of Fig. 1. Then, in Sec. III B, we present analytical results based on the simplified hair cell equation (5) which give additional insights.

A. Numerical computations

The cilia displacement u is first determined using the analytical theory outlined in Sec. I. Equation (3) is then solved numerically as follows. The periodic response is computed directly and efficiently by first determining the initial conditions which eliminate the transient portions of the response. This is accomplished by writing the solution in terms of an integrating factor with definite integrals and one undetermined constant of integration which represents the initial condition (Boyce and Diprima, 1977). The definite integrals involved are computed numerically and the constant is then evaluated by requiring that the solution be periodic.

1. The ac responses

The peak-to-peak hair cell potential as a function of frequency exhibits significant changes for the different stapes amplitudes of Fig. 7(b). We first consider the changes in the isointensity response generated at each stage in the model (Fig. 1) and then discuss the effect of stapes amplitude on the final output.

The isointensity response of the basilar membrane [in

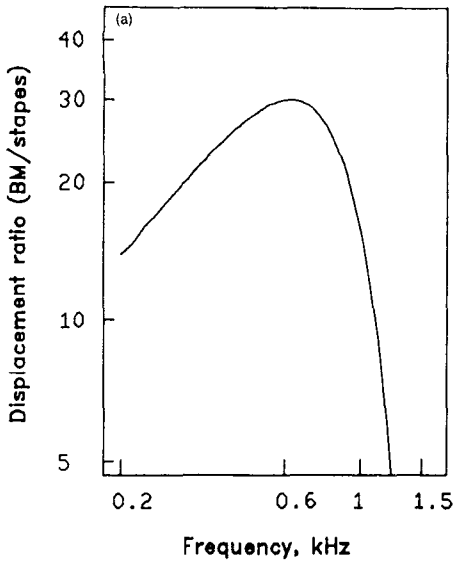

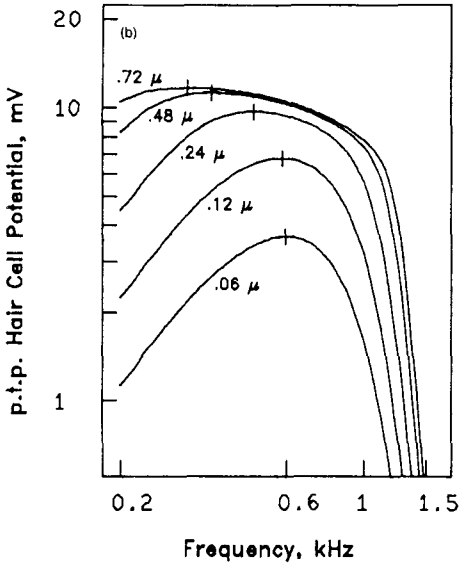

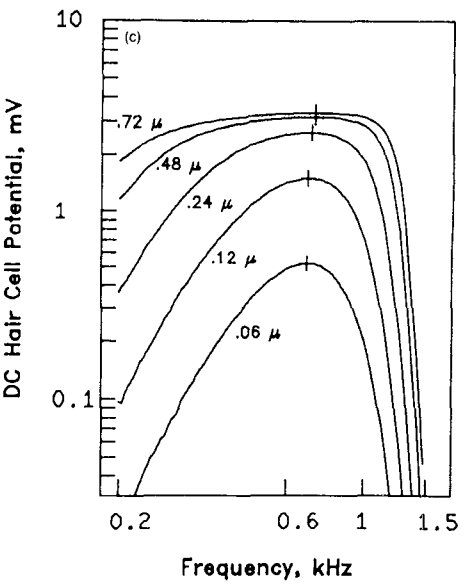

FIG. 7. (a) Peak basilar membrane displacement versus frequency at a constant stapes amplitude = 0.1 μm and a fixed location $s_0 = 0.65$. (b) ac transfer characteristics of the composite model. Each curve represents the peak-to-peak intracellular potential versus frequency of sinusoidal stapes displacement presented at a certain maximum displacement level (indicated by the associated parameter) and a fixed location $s_0 = 0.65$. (c) dc transfer characteristics of the composite model. Each curve represents the average intracellular potential (deviation from rest) versus frequency of sinusoidal stapes displacement presented at a certain maximum displacement level (indicated by the associated parameter) and a fixed location $s_0 = 0.65$.

Figs. 1(a) and 7(a)] is filtered by the transfer function of the fluid–cilia coupling stage which results in a steeper low-frequency slope and an upward shift in the frequency of the peak response.[3] These effects are expected to be larger in more apical hair cells (i.e., larger s) since their BF approaches that of the cutoff frequency of the fluid–cilia coupling filter stage (550 Hz) and the isointensity response of the basilar membrane becomes progressively less tuned. Because of *linear* basilar membrane mechanics and fluid–cilia coupling, this upward BF shift is independent of stapes amplitude. Amplitude dependence in the model is first exhibited at the next stage, in which the isointensity response of the cilia displacement is flattened by the hair cell saturating nonlinearity [Fig. 1(c)]. For large stapes amplitude a significant frequency range is affected and hence the response appears less tuned. The final stage is low-pass filtering [Fig. 1(d)] which steepens the high-frequency slope and shifts the BF downward. Note, however, that at significantly higher frequencies (>3–4 kHz), where the basilar membrane frequency response is expected to be sharper, the downward BF shifts may decrease. The amount of downward shift increases with larger basilar membrane amplitudes as the hair cell response becomes more saturated and less tuned, especially for locations for which the BF lies in the frequency range where the low-pass slope is steepest.

There are then two sources for the BF shifts. The first is independent of stapes amplitude. It is attributable to the action of the linear cascade of filters (upwards by the high pass of the fluid–cilia coupling and downwards by the low pass of the hair cell). These BF shifts are influenced by the broadness of the basilar membrane tuning in the low-frequency region of the cochlea. They may be significantly reduced in this region if we include the overall effects of the middle ear low-pass filter (Flanagan, 1972) which further steepens the high-frequency slopes of the basilar membrane tuning curves beyond the 6-dB/oct slopes of the cascade of filters. The second source of BF shifts (on which we will concentrate in the remainder of this report) is nonlinear and is strongly dependent on the action of the hair cell saturating nonlinearity and low-pass filter. It manifests itself in the isointensity curves at higher amplitudes as downward BF shifts and increasing bandwidth of the response.

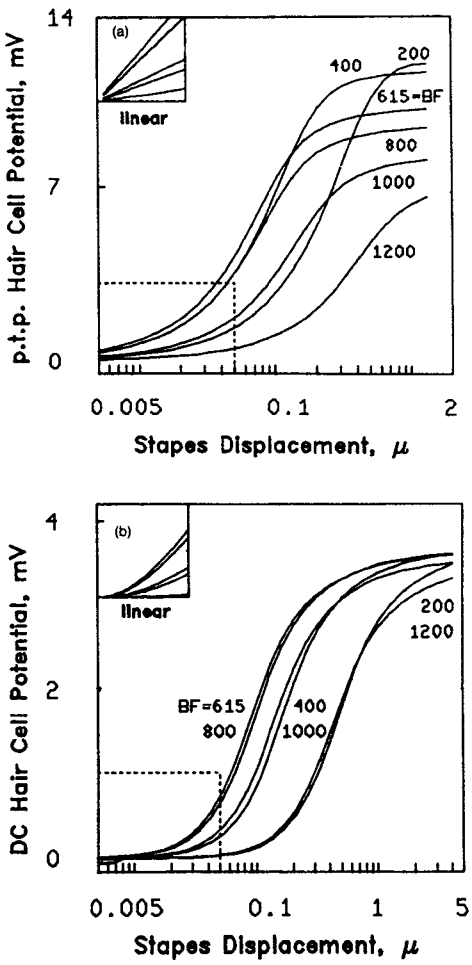

FIG. 8. (a) The ac hair cell potential (peak to peak) versus stapes displacement with frequency as a parameter. The inset is a replot with linear axes of the curve segments contained within the dashed box. It shows the linear dependence of the ac potential on stapes amplitude at low levels of intensity. (b) Average dc hair cell potential (deivation from rest) versus stapes displacement with frequency as a parameter. The inset is a replot with linear axes of the curve segments contained within the dashed box. It shows the quadratic dependence of the dc potential on stapes amplitude at low levels of intensity.

These amplitude-dependent changes of the response are shown in the computed ac responses of Fig. 7(b). At the highest intensity the frequency response between 200–1000 Hz [at Fig. 1(d)] is significantly saturated and appears almost flat to the hair cell low-pass filter; the overall ac response then resembles that filter's transfer function (Fig. 6).

A second characterization of the response is the ac response versus stapes amplitude with frequency as a parameter [Fig. 8(a)]. These ac functions show several features. The peak-to-peak level saturates and the level of saturation decreases with increasing frequency. This occurs because first the asymptotic (for large u) maximum and minimum values of hair cell conductance are limited by the saturating $g(u)$ and then the low-pass filter attenuates the ac output waveform more severely for higher frequencies. The BF curve is therefore the leftmost curve for small displacements but not for larger displacements.

2. The dc responses

There are significant differences between the ac and dc measures of hair cell output. First, because of the linearity of the basilar membrane model, the dc components in the response waveforms appear only *after* and as a result of the hair cell asymmetrical nonlinearity. The larger the basilar membrane displacement the more dc is generated. Second, the low-pass filter stage does not affect the dc measure. The dc outputs therefore do not show any downward shifts relative to basilar membrane BF, but rather upward shifts due to the fluid–cilia coupling. As in the case of the ac responses, this BF shift (relative to that of the basilar membrane) at small stapes amplitude is related to the broadness of the basilar membrane tuning curve. In the range of low intensities [where Eq. (5) is a good approximation] the BF remains fixed as intensity is varied. At higher intensities, however, the model solutions [computed from the more complete Eq. (3)] show some small upward shifts [Fig. 7(c)]. Note that the low-frequency slopes of the dc curves are steeper than the corresponding ac and basilar membrane curves (e.g., for the 0.06 μ maximum displacement curves, the slope of the ac curve is $\approx$13 dB/oct in the 200–400-Hz region, whereas the slope of the dc curve is $\approx$18 dB/oct); this sharpening effect is attributed to the hair cell nonlinearity (see the analytical results in Sec. III B).

In Fig. 8(b) the dc response is plotted versus stapes amplitude with frequency as a parameter. As in the ac case the BF curve is leftmost; here, this is true for almost the entire range of displacements. In addition, the saturating levels of these curves show relatively small dependence on frequency.

B. Analytical results

For a pure tone with angular frequency ω, the cilia displacement is given as

$$u(t,s) = u_m(\omega,s)\sin[\omega t + \Phi(\omega,s)], \qquad (6)$$
$$u_m = I_0 Am(\omega,s).$$

Here I_0 denotes stapes amplitude, $Am(\omega,s)$ is the product of the magnitude of the transfer functions for the basilar membrane and fluid–cilia coupling, and $\Phi(\omega,s)$ is the sum of their respective phases. In terms of the dimensionless cilia displacement $y = u/u_m$, scaled so that $-1 \leqslant y \leqslant 1$, the displacement-dependent conductance function in Eq. (5) takes the form

$$g(y) = \tilde{g}(u_m y) = e^{\alpha y}/(1+\beta e^{\alpha y}) - 1/(1+\beta), \qquad (7)$$

where $\alpha = u_m/(RT/Z_1)$; α is a dimensionless parameter measuring the degree of nonlinearity in $g(y)$.

Here we shall concentrate on asymptotic solutions of Eq. (5) for large and small α. We note that for large α, $g(y)$ is asymptotically an asymmetrical step function:

$$g(y) \equiv g_u = 1/[\beta(\beta+1)], \quad 0 < y \leqslant 1, \qquad (8)$$
$$g(y) \equiv g_l = -1/(1+\beta), \quad -1 \leqslant y < 0,$$

while for small α, $g(y)$ is a linear function with correction terms

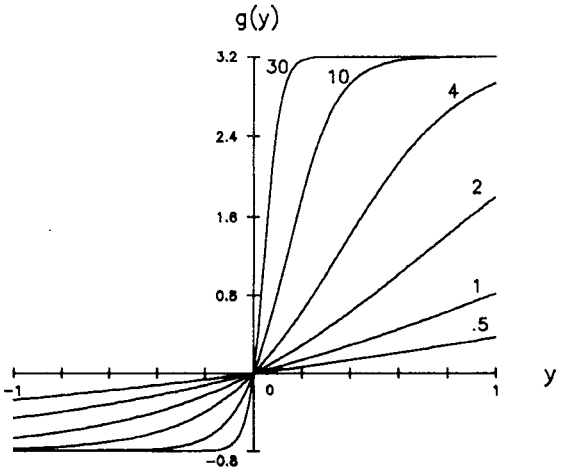

FIG. 9. Normalized hair cell conductance as a function of normalized cilia displacement. Equation (7) is plotted with $\beta = \frac{1}{4}$ and α as a parameter whose values label the different curves. The conductance is almost linear for $\alpha < 1$; for large values of α the conductance approaches an asymmetrical step function.

$$g(y) = [\alpha/(1+\beta)^2]y + [(1-\beta)\alpha^2/2(1+\beta)^3]y^2 + \cdots . \quad (9)$$

The function $g(y)$ is plotted in Fig. 9 to show the transition from linear to steplike behavior with increasing amplitude.

1. Hair cell dc response

For a pure tone, the dc response can be found by integration of Eq. (5) over a complete cycle. After a change of variable, $y = \sin(t)$, we obtain

$$v_{dc} = \pi^{-1}\int_{-1}^{1} \frac{g(y)}{\sqrt{(1-y^2)}dy}. \quad (10)$$

For large α, we use the step function approximation to $g(y)$ given by Eq. (8) to obtain

$$v_{dc} = (g_u + g_l)/2 + O(\alpha e^{-\alpha}). \quad (11)$$

Thus the dc response saturates to the mean value of the input (i.e., dimensionless conductance in this scaling and approximation) for large enough stapes amplitudes independent of frequency. For the parameter values used in Fig. 8(b), v_{dc} in dimensional form takes the value 3.87 mV, which differs only slightly from the asymptotes in Fig. 8(b); this difference is due primarily to approximating Eq. (3) by Eq. (5).

For small α, we use Eq. (9) to approximate the conductance in Eq. (10). By symmetry, the linear term does not contribute to the integral. This is expected since a linear conductance–displacement relation should not produce a dc response. The quadratic term does contribute, however:

$$v_{dc} = (\tfrac{1}{4})[(1-\beta)/(1+\beta)^3]\alpha^2 + O(\alpha^4). \quad (12)$$

This is an interesting result in that for small amplitudes, the dc response is proportional to the square of $Am(\omega,s)$, and hence sharper than the mechanical response. This effect can be seen when comparing Fig. 7(a) (note linear scale) with Fig. 7(c). Equation (12) also explains the parabolic behavior of the curves near the origin of Fig. 8(b) (see inset).

2. Hair cell ac response

The voltage waveform near saturation is obtained by integration of Eq. (5) using Eq. (8) to approximate the conductance. The result is expressed in terms of the exponentials:

$$v(\theta) = g_u + (v_0 - g_u)e^{-\theta/\omega\tau}, \quad 0 \leqslant \theta \leqslant \pi,$$
$$= g_l + D_0 e^{-(\theta-\pi)/\omega\tau}, \quad \pi \leqslant \theta \leqslant 2\pi, \quad (13)$$

where θ is the phase measured relative to the cilia displacement and $v_0 = v(0)$. The constant D_0 is formed by requiring continuity at $\theta = \pi$,

$$D_0 = (g_u - g_l) + (v_0 - g_u)e^{-\pi/\omega\tau} \quad (14)$$

and v_0 is found from the periodicity condition $v(0) = v(2\pi)$,

$$v_0 = g_u - (g_l - g_u)(1 - e^{-\pi/\omega\tau})/(1 - e^{-2\pi/\omega\tau}). \quad (15)$$

These relations predict the waveforms shown in Fig. 5(b). The peak-to-peak response is

$$v_{ac} = v(\pi) - v_0(1/\beta)(1 - e^{-\pi/\omega\tau})^2/(1 - e^{-2\pi/\omega\tau}). \quad (16)$$

At low frequencies $v_{ac} \sim 1/\beta = g_u - g_l$, while at high frequencies $v_{ac} \sim \pi/(2\beta\omega\tau)$. Thus the frequency response is that of a low-pass filter with a high-frequency slope of -6 dB/oct. This behavior is also shown in the computed frequency response for large amplitudes shown in Fig. 7(b). It is worth noting that more accurate representations of the waveform have been obtained for large α. In the neighborhood of $\theta = 0,\pi$ the approximation of Eq. (8) breaks down. Transition layer expressions constructed for these regions can be asymptotically matched to the given solution. These corrections smooth the sharp corners of the waveform at $\theta = 0,\pi$.

For small amplitudes, the voltage waveforms are nearly sinusoidal. Using Eq. (9) to approximate the conductance, the solution of Eq. (5) can be written as a sum of a dc component and oscillatory terms having frequencies ω, 2ω, 3ω,... . The magnitude of the fundamental is

$$\alpha[1 + (\omega\tau)^2]^{-1/2}/(1+\beta)^2 + O(\alpha^3). \quad (17)$$

For small amplitudes this closely approximates the peak-to-peak response, and explains the low amplitude behavior in Fig. 7(b) as essentially the product of the basilar membrane, fluid–cilia coupling, and linearized hair cell transfer functions. In Fig. 8(a) the large stapes amplitude behavior is adequately given by Eq. (16), while the linear behavior at small amplitudes is explained by Eq. (17).

IV. DISCUSSION

The model presented in this report is a minimal synthesis of the various stages of cochlear processing. It consists of three primary components: a linear basilar membrane, a linear fluid–cilia coupling stage, and an inner hair which incorporates a saturating nonlinearity due to the transduction process. The parameters of the model have reasonable physiological interpretations and their numerical values are derived when possible from published experimental measure-

ments. The mathematical treatment of the model results in relatively simple equations that allow an intuitive and analytical understanding of the numerically computed solutions. The present analysis of the model is restricted to frequencies below 1.5 kHz. We will first discuss the results of our model in light of comparable experimental data and then interpret them from the point of view of the tonotopic code and its intensity invariance.

The computed responses to single tone inputs fall in the physiologic range and display the major qualitative features of hair cell intracellular potentials and auditory nerve fiber activity such as frequency tuning (Fig. 7), rectified waveforms (Fig. 5) (Hudspeth and Corey, 1977), and saturating rate-level and synchrony-level functions (Fig. 8) (Kiang 1965, 1980; Rose *et al.*, 1967, 1971; Russell and Sellick, 1978; Sellick and Russell, 1980).

The computed results also account for two experimentally observed effects of the stimulus intensity of the frequency tuning of ac response measures. The first effect is the broadening of the response bandwidth with increasing sound intensity (Dallos and Santos-Sacchi, 1983), a trend which, in our model [Fig. 7(b)], is caused by the saturating nonlinearity. The second effect of increasing stimulus intensity is the downward shift of the BF of the hair cell recorded ac response (Dallos and Santos-Sacchi, 1983). This shift is present in the computed responses [Fig. 7(b)] and can be traced to the combined influences of the nonlinearity and of the low-pass action of hair cell capacitive membranes. While our calculated responses show qualitative agreement with the experimental data of Dallos and Santos-Sacchi (1983), the sharper second peak shown in their Fig. 2 is not reproduced in the present model, and often does not appear in their data (Dallos, 1984). We note that the bandwidth broadening and BF shifts have also been observed in the phase locked responses of auditory nerve fibers (BF$\geqslant$1000 Hz) in experiments using noise stimuli and reverse correlation methods to obtain the fibers' "transfer functions" (Evans, 1977; Harrison and Evans, 1982; Moller, 1978; Moller 1983a,b).

The model's dc isointensity curves also display a bandwidth increase with intensity. However, unlike the ac response, the peaks of the dc response curves do not shift downwards, but rather slightly upwards [Fig. 7(c)]. Similar behavior is observed in recorded isointensity responses of auditory nerve fibers using average rate measures of the activity (Kiang, 1980; Moller, 1983a).

It is difficult to compare directly our computed responses versus stapes amplitude functions [Fig. 8(a),(b)] with experimental data, since there is a lack of recordings of hair cell ac and dc potentials versus sound intensity in cochlear apical units with BF's below 1.5 kHz (the frequency range of our model). Our computed functions [Fig. 8(a),(b)] nevertheless resemble functions recorded in hair cells of the basal turn of the cochlea (responding to low-frequency tones) (Patuzzi and Sellick, 1983; Russell and Sellick, 1978; Sellick and Russell, 1979) and in auditory nerve fibers (Kiang, 1980). In particular, the saturating ac functions reproduce two experimentally observed features: (1) decreasing saturation levels with increasing frequency, which we attribute to the combined effect of the saturating nonlinearity followed by the hair cell low-pass filter and (2) horizontal positioning for different frequencies which reflects the frequency tuning of the cascade (i.e., for low intensity, the BF curve is leftmost). The computed dc functions also display such horizontal positioning, but a relatively weak saturation level dependence on frequency. This also agrees with experimental measurements (both at the hair cell and auditory nerve fiber levels) at frequenices below the BF of the unit (Sachs and Abbas, 1974; Evans, 1975; Patuzzi and Sellick, 1983).

The only nonlinearity considered in the present composite model is that of the hair cell transduction process. The asymmetry in the form of this nonlinearity is crucial to the generation of the dc responses and is responsible for their quadratic dependence on the stapes amplitude (in contrast to the linear dependence of the ac response) at low intensities (Fig. 8). This type of dependence, which has been predicted earlier in phenomenological models (Engebretson and Eldredge, 1968) and recently demonstrated experimentally (Patuzzi and Sellick, 1983), explains the sharper low-frequency slopes of the isointensity dc response curves [Fig. 7(c)] compared to those of the ac response curves [Fig. 7(b)].

There is at present a considerable variety of views about the nature and extent of nonlinearities in basilar membrane motion and fluid–cilia coupling mechanisms (Chadwick *et al.*, 1980; Evans, 1975; Holton and Weiss, 1983a,b; Kim and Molnar, 1975; Palmer and Evans, 1980; Patuzzi and Sellick, 1983; Rhode, 1971; Sellick *et al.*, 1983; Transcripts, 1980). We have elected to use a linear basilar membrane model since it affords a great deal of mathematical tractability and physiological relevance without sacrificing the major observed qualitative features of basilar membrane motion (Chadwick *et al.*, 1980). Nonlinear mechanisms for the generation of hair cell potentials and nerve spike trains, considered here and in other theoretical studies (Engebretson and Eldredge, 1968; Pfeiffer, 1970; Schroeder and Hall, 1974) have been shown capable of accounting for the various nonlinear phenomena such as two-tone suppression, saturation, and rectification. However, propagating combination tones (Kim *et al.*, 1980) and the possible active tuning (Kim, 1980; Siegel and Kim, 1982; Weiss, 1982) are two phenomena that could involve nonlinearities at the basilar membrane (or its coupling properties to the hair cells). Some descriptive models without explicit biophysical components have been proposed to account for these phenomena (de Boer, 1983; Neely and Kim, 1982). However, to explore adequately a variety of mechanisms in the context of our physiological approach is beyond the scope of this paper.

We finally discuss aspects of the experimental identification of a unit's BF, and the consequences of the intensity and stage-dependent BF shifts for this identification and more generally for the interpretation of a place or tonotopic code. In the traditional view of the place code there exists a one-to-one correspondence between the frequency of a pure tone and the spatial location of maximal mechanical and electrical response along the cochlear partition. By inverting this mapping we may associate with each location a frequen-

cy which is referred to here as the *global BF*. The experimental determination of the global BF is difficult (Pfeiffer and Kim, 1975) and so an alternate measurement has been widely made using swept tones. In this method the BF for a specific location is identified from the maximum of the isointensity response curve (which agrees at low intensities with the BF from the minimum of the threshold tuning curve). A BF determined using swept tones will be referred to here as a *local BF*. In general, the global and local BF's are not the same and both may be stage and intensity dependent. In our model, the local BF varies with stage and intensity whereas the global BF does not. The stage dependence of the local BF results from the combined effects of the high-pass filter in the fluid–cilia coupling stage and the low-pass action of the hair cell membranes. The intensity dependence results from the nonlinear conductance–displacement relation in the hair cell. In contrast, the global BF in our model does not depend on either stage or intensity. It is stage invariant because the mechanical and electrical parameters of the hair cells and fluid–cilia coupling are independent of s, and because its determination involves a single frequency; it is intensity invariant because the nonlinearity acts only after any s-dependent stages that may occur.[4] In theory and experiment one may find the consequences of such BF shifts. The isointensity ac response may sometimes bear little relationship to the global tuning of the basilar membrane. An extreme case in point here is the hair cells of the basal turn, which show larger ac responses for an 80 dB SPL tone at 6 kHz than at their nominal BF (e.g., 17 kHz) [Russell and Sellick, 1978, Fig. 3(d)]. On the other hand, a local BF determined from a hair cell dc response curve could be close to the corresponding global BF, particularly at low intensities and away fron the apical end where mechanical tuning is broad. All these discrepancies between the global BF and its local measurement become smaller for sharper basilar membrane tuning.

For a tonotopic code to provide information that is easily interpreted by the brain, it would seem desirable that a one-to-one correspondence between place (or auditory nerve fiber identity) and global BF be preserved under intensity changes. This is what we mean by tonotopic intensity invariance. In this sense the present model is tonotopically invariant, as would be any model based upon linear mechanics and a monotonic nonlinear hair cell electrodynamics which is s independent. A system with significant mechanical nonlinearity or significant spatial dependence in nonlinear properties in latter cochlear stages would likely not exhibit tonotopic invariance. In such cases, one has to conclude either that the tonotopic map of the auditory system is not used to derive the relatively invariant pitch percepts, or that complex central auditory mechanisms exist which would unravel the global BF shifts to deduce unambiguously the stimulus intensity and frequency characteristics.

The above considerations largely carry through to the case of complex sounds where, in addition, other effects have to be considered, such as the generation of distortion products, and synchrony and rate suppression (Young and Sachs, 1979).

APPENDIX: EQUATIONS FOR BASILAR MEMBRANE MOTION

Explicit relations are given here that describe the response (displacement w) of the basilar membrane model to a pure tone when the frequency is less than 1500 Hz. The relations given below are intended to provide interested readers with an explicit, self-contained computational recipe that is previously unpublished. The definitions of the variables and parameters are summarized in Table AI. The formulas incorporate spatially variable basilar membrane width, thickness, and cross-sectional chamber dimensions. The edges of the membrane are simply supported, and the shape of a chamber is a rectangle with width: height in the ratio 2:1.

$$w(s,x,T) = -(8/\pi)\rho^{1/2}B^{5/2}D_0^{-1/2}\Omega d_s \times A_r \cos[\pi x/2F(s)] \times \mathrm{Re}\left(\frac{P(s)\exp(i\Omega T)\sin(\epsilon^{-1}\int_1^s k(s')ds')}{f(s)\cos(\epsilon^{-1}\int_0^1 k(s')ds')}\right), \quad \text{(A1)}$$

$$k(s) = \alpha_0^{-1/2}k_0(s) + \alpha_0^{-3/2}k_1(s), \quad \text{(A2)}$$

$$k_0^2(s) = 16F(s)\{\pi^2 H^2(s)[1-3\delta(s)]f(s)\}^{-1}, \quad \text{(A3)}$$

TABLE AI. Definition of quantities used in basilar membrane model.

A	=	scaled chamber area (dimensionless)
A_r	=	ratio of oval window area to chamber area at basal end (dimensionless)
B	=	maximum basilar membrane half-width (cm), used to scale cross-plane dimensions
C_0	=	partition damping constant (dimensionless), $C'B^4/D_0$
C'	=	dimensional damping constant (dyn/cm^3)
d_s	=	stapes amplitude (cm)
D_0	=	maximum basilar membrane bending stiffness (dyn-cm)
D	=	scaled bending stiffness function (dimensionless)
F	=	scaled basilar membrane half-width (dimensionless)
h	=	scaled basilar membrane thickness (dimensionless)
h_0	=	maximum basilar membrane thickness (cm)
H	=	scaled chamber height (dimensionless)
i	=	$\sqrt{-1}$
k	=	scaled wavenumber (dimensionless)
L	=	length of basilar membrane (cm), used to scale longitudinal dimension
M_0	=	basilar membrane mass parameter (dimensionless), equal to $\mu B^4\Omega^2/D_0$
M	=	basilar membrane mass function (dimensionless)
P	=	scaled chamber perimeter (dimensionless)
s	=	longitudinal coordinate, scaled by L (dimensionless), see Fig. 2(a)
T	=	time (s)
w	=	basilar membrane displacement (cm)
x	=	transverse coordinate, scaled by B (dimensionless), see Fig. 2(a)
α_0	=	$D_0/(\rho B^5\Omega^2)$ frequency expansion parameter (dimensionless)
ϵ	=	B/L slenderness ratio
μ	=	characteristic mass/area (g/cm^2) of basilar membrane partition used in definition of M_0, equal to basilar membrane density times h_0
ν	=	kinematic viscosity (cm^2/s)
ρ	=	fluid density (g/cm^3)
Ω	=	angular frequency (rad/s)

TABLE AII. Correspondence in notation.

Present	(Chadwick, 1985)
$F(s)$	$G(x)$
s	x
x	y
α_0	α
C_0 (damping constant)	not used
not used	C_0 (constant pertaining to stapes amplitude)

$$\delta(s) = (i\Omega B^2/\nu)^{-1/2}/H(s), \tag{A4}$$

$$f(s) = D(s)\{\pi/[2F(s)]\}^4 - M_0 M(s) + i\Omega C_0, \tag{A5}$$

$$\frac{k_1(s)}{k_0(s)} = \frac{32F(s)[1 + (5/2)\delta(s)]}{[9\pi^2 f(s)]} + \frac{\delta(s)}{[3H(s)]} \sum_{m=1}^{\infty} \frac{(-1)^m B_m(s)}{\gamma_m(s)} - \frac{5\pi}{18} \sum_{m=1}^{\infty} B_m(s) K_m(s) \coth[\gamma_m(s) H(s)], \tag{A6}$$

$$\gamma_m(s) = m\pi/H(s); \quad m = 1,2,\ldots, \tag{A7}$$

$$K_m(s) = \frac{\pi}{2F^2(s)} \frac{\cos[\gamma_m(s)F(s)]}{[\pi/2F(s)]^2 - \gamma_m^2(s)} \quad \text{if } \gamma_m \neq \frac{\pi}{(2F)},$$

$$K_m(s) = \tfrac{1}{2} \quad \text{if } \gamma_m = \pi/(2F) \tag{A8}$$

$$B_m(s) = -\{16/[H(s)F(s)f(s)\gamma_m(s)]\}K_m(s), \tag{A9}$$

$$P(s) = (2k_0(s)H^2(s)\{1 - \alpha_0^{-2}[k_1(s)/k_0(s)]^2\})^{-1/2}. \tag{A10}$$

These formulas are based on a theory (Chadwick, 1985) that utilizes the WKB approximation applied to a three-dimensional model, and then uses further asymptotics in the cross plane to determine the wavenumber explicitly. Several notational changes had to be made here that should be noted when referring to (Chadwick, 1985). These are given in Table AII.

[1]References in this paper to the apical portion or apical membrane of the hair cell are meant to include the membrane of the cilia since the exact location of the mechanically sensitive channels is at present still uncertain.

[2]The parameter values shown in Table I are estimated to be within the physiologic range for a diverse set of experimental conditions and hence are not intended to duplicate accurately any particular preparation. The hair cell model presented in this report is quite robust in that the observed features of the computed responses do not critically depend on any one or set of parameter values. For the basilar membrane, care was taken to make sure that all parameters are consistent. For example, L, B, F, h_0, h, and H are all derived from Fernandez (1952) on the guinea pig, and D_0 was selected by fitting the model to low-frequency guinea pig data obtained by von Békésy (1960). However, lack of adequate experimental data necessitates the approximation of certain parameters, such as ρ. These were chosen to be within reasonable physiological ranges.

[3]Hereafter we shall refer to the frequency of peak response as the best frequency, BF. Note, however, that in general this definition depends on both stage and amplitude. Our presentation shall make this distinction explicit if the context does not clearly reveal it.

[4]These conclusions on global BF invariance can be understood as follows. For a fixed frequency, consider the input–output properties of the feedforward cascade. The amplitude of the hair cell response $\mathbf{H}$ is a nonlinear function of the cilia displacement which itself is represented as the product of intensity I_0 with the transfer functions $\mathbf{F}$ and $\mathbf{B}(s)$ of the fluid–cilia and basilar membrane stages, respectively: $\mathbf{H} = \mathbf{H}[I_0,\mathbf{F},\mathbf{B},(s)]$. Global BF derives from the value of s where $\mathbf{H}$ reaches a maximum, i.e., by the chain rule, s must satisfy $0 = \partial\mathbf{H}/\partial s = \mathbf{H}'\cdot I_0\cdot\partial\mathbf{B}/\partial s$, where $\mathbf{H}'$ is the derivative of $\mathbf{H}$ with respect to its argument. Note that, since the hair cells are identical, $\mathbf{H}$ does not depend explicitly on s. Thus when $\mathbf{H}$ is monotonic (i.e., $\mathbf{H}' \neq 0$), as in our case, the global BF is determined by $\mathbf{B}$ and is independent of I_0. Note that the I_0 independence would still hold even if cilia properties ($\mathbf{F}$) depend on s.

Allen, J. B. (1980). "A cochlear micromechanical model of transduction," Proceedings of the 5th International symposium on Hearing (Delft U. P., The Netherlands), pp. 85–95.

von Békésy, G. (1960). *Experiments in Hearing* (McGraw-Hill, New York).

de Boer, E. (1983). "Power amplification in an active model of the cochlea-short-wave case," J. Acoust. Soc. Am. **73**, 577–579.

Boyce, W. E., and Diprima, R. C. (1977). *Elementary Differential Equations and Boundary Value Problems* (Wiley, New York), pp. 15–16.

Chadwick, R. S. (1985). "Three dimensional effects on low frequency cochlear mechanics," Mech. Res. Comm. **12**, 181–186.

Chadwick, R. S., and Cole, J. D. (1979). "Modes and waves in the cochlea," Mech. Res. Comm. **6**(3), 177–184.

Chadwick, R. S., Fourney, M. E., and Neiswander, P. (1980). "Modes and waves in a cochlear model," Hear. Res. **2**, 475–483.

Corey, D. P., and Hudspeth, A. J. (1983a). "Analysis of the microphonic potential of the bullfrog's sacculus," J. Neurosci. **3** (5), 942–961.

Corey, D. P., and Hudspeth, A. J. (1983b). "Kinetics of the receptor current in bullfrog saccular haircell," J. Neurosci. **3** (5), 962–976.

Dallos, P. (1984). Personal communication.

Dallos, P. (1973). *The Auditory Periphery* (Academic, New York).

Dallos, P., and Santos-Sacchi, J. (1983). "AC receptor potentials from hair cells in the low-frequency region of the guinea pig cochlea," in *Mechanisms of Hearing*, edited by W. Webster and L. Aitkin (Monash U. P., Australia).

Dallos, P. (1983). "Some electrical circuit properties of the organ of Corti. I. Analysis without reactive elements," Hear. Res. **12**, 89–119.

Davis, H. (1965). "A model for transducer action in the cochlea," Cold Spring Harbor Symp. Quant. Biol. **30**, 181–190.

Engebretson, A. M., and Eldredge, D. (1968). "Model for nonlinear characteristics of cochlear potentials," J. Acoust. Soc. Am. **44**, 548–554.

Evans, E. F. (1975). "Cochlear nerve and cochlear nucleus," in *Handbook of Sensory Physiology, Vol. 2* (Springer, Berlin), pp. 1–108.

Evans, E. F. (1977). "Frequency selectivity at high signal levels of single units in cochlear nerve and nucleus," in *Psychophysics and Physiology of Hearing*, edited by E. F. Evans and J. P. Wilson (Academic, New York), pp. 185–192.

Fernandez, C. (1952). "Dimensions of the cochlea (guinea pig)," J. Acoust. Soc. Am. **24**, 519–523.

Flanagan, J. L. (1972). *Speech Analysis Synthesis and Perception* (Springer, Berlin).

Flock, A., and Strelioff, D. (1984). "Studies on haircells in isolated coils from the guinea pig cochlea," Hear. Res. **15**, 11–18.

Harrison, R. V., and Evans, E. V. (1982). "Reverse correlation study of cochlear filtering in normal and pathalogical guinea pig ears," Hear. Res. **6**, 303–314.

Holmes, M., and Cole, J. (1984). "Cochlear mechanics: Analysis for a pure tone," Dep. Math. Sci., Rensselaer Polytech. Inst., Troy, N. Y. (AD-A13643819).

Holton, T., and Weiss, T. F. (1983a). "Receptor potentials of lizard cochlear hair cells with free-standing stereocilia in response to tones," J. Physiol. **345**, 205–240.

Holton, T., and Weiss, T. F. (1983b). "Frequency selectivity of hair cells and nerve fibers in the alligator lizard cochlea," J. Physiol. **345**, 241–260.

Hudspeth, A. J., and Corey, D. P. (1977). "Sensitivity, polarity, and conductance change in the response of vertebrate hair cells to controlled mechanical stimuli," Proc. Nat. Acad. Sci. **74**(6), 2407–2411.

Kiang, N. Y. (1965). "Discharge patterns of single fibers in the cat's auditory nerve," Res. Mono. No. 35 (MIT, Cambridge, MA).

Kiang, N. Y. (1980). "Processing of speech by the auditory nervous system," J. Acoust. Soc. Am. **68**, 830–835.

Kim, D. O. (1980). "Cochlear mechanics: Implications of electrophysiolo-

gical and acoustical observations," Hear. Res. **2**, 297–317.
Kim, D. O., and Molnar, C. E. (**1975**). "Cochlear mechanics: Measurements and models," in *The Nervous System, Vol. 3*, edited by D. B. Tower (Raven, New York), pp. 57–68.
Kim, D. O., Molnar, C. E., and Matthews, J. W. (**1980**). "Cochlear mechanics: Nonlinear behavior in two-tone responses as reflected in cochlear-nerve-fiber responses and in ear-canal sound pressure," J. Acoust. Soc. Am. **67**, 1704–1721.
Lewis, R. S., and Hudspeth, A. J. (**1983**). "Voltage- and ion-dependent conductances in solitary vertebrate hair cells," Nature **304**, 538–541.
Moller, A. R. (**1978**). "Frequency selectivity of the peripheral auditory analyzer studied using broad band noise," Acta Physiol. Scand. **104**, 24–32.
Moller, A. R. (**1983a**). "Frequency selectivity of phase-locking of complex sounds in the auditory nerve of the rat," Hear. Res. **11**, 267–284.
Moller, A. R. (**1983b**). "Use of pseudorandom noise in studies of frequency selectivity: the periphery of the auditory system," Biol. Cybern. **47**(2), 95–102.
Morrish, K. A., Chadwick, R. S., Shamma, S. A., and Rinzel, J. (**1986**). "Parameter sensitivity in a mathematical model of basilar membrane mechanics," in *Peripheral Auditory Mechanisms*, edited by J. B. Allen, J. L. Hall, A. Hubbard, S. T. Neely, and A. Tubis (Springer, New York).
Neely, S. T., and Kim, D. O. (**1982**). "An active cochlear model shows sharp tuning and high sensitivity," Hear. Res. **9**, 123–130.
Palmer, A. R., and Evans, E. F. (**1980**). "Cochlear fiber rate-intensity functions: no evidence for basilar membrane nonlinearities," Hear. Res. **2**, 319–326.
Patuzzi, R., and Sellick, P. M. (**1983**). "Basilar membrane motion and inner hair cell output," J. Acoust. Soc. Am. **74**, 1734–1741.
Pfeiffer, R. (**1970**). "A model for two-tone inhibition of single cochlear-nerve fibers," J. Acoust. Soc. Am. **48**, 1373–1378.
Pfeiffer, R., and Kim, D. (**1975**). "Cochlear nerve fiber responses: Distribution along the cochlear partition," J. Acoust. Soc. Am. **58**, 867–869.
Rhode, W. S. (**1971**). "Observations of the basilar membrane in squirrel monkey using the Mossbauer technique," J. Acoust. Soc. Am. **49**, 1218–1231.
Rose, J. E., Brugge, J. F., Anderson, D. J., and Hind, J. E. (**1967**). "Phase-locked responses to low frequency tones in single auditory nerve fibers of the squirrel monkey," J. Neurophysiol. **30**, 769–792.
Rose, J. E., Hind, J. E., Anderson, D. J., and Brugge, J. F. (**1971**). "Some effects of stimulus intensity on response of auditory nerve fibers in the squirrel monkey," J. Neurophysiol. **34**, 685–699.
Russell, I. J., and Sellick, P. M. (**1978**). "Intracellular studies of hair cells in the mammalian cochlea," J. Physiol. (London) **284**, 261–290.
Russell, I. J. (**1983**). "Origin of the receptor potential in inner hair cells of the mammalian cochlea—evidence for Davis' theory," Nature **301** (27), 334–336.
Sachs, M., and Abbas, P. (**1974**). "Rate versus level functions for auditory-nerve fibers in cats: Tone-bursts stimuli," J. Acoust. Soc. Am. **56**, 1835–1847.
Schroeder, M., and Hall, J. (**1974**). "A model for mechanical to neural transduction in the auditory receptor," J. Acoust. Soc. Am. **55**, 1055–1060.
Sellick, P. M., and Russell, I. J. (**1979**). "Two-tone suppression in cochlear hair cells," Hear. Res. **1**, 227–236.
Sellick, P. M., and Russell, I. J. (**1980**). "The responses of inner hair cells to basilar membrane velocity during low frequency auditory stimulation in the guinea pig cochlea," Hear. Res. **2**, 439–445.
Sellick, P. M., Patuzzi, R., and Johnstone, B. (**1982**). "Modulation of responses of spiral ganglion cells in the guinea pig cochlea by low frequency sound," Hear. Res. **7**, 199–221.
Sellick, P. M., Patuzzi, R., and Johnstone, B. (**1983**). "Comparison between the tuning properties of inner hair cells and basilar membrane motion," Hear. Res. **10**, 93–100.
Siegel, J. H., and Kim, D. O. (**1982**). "Efferent neural control of cochlear mechanics? Olivocochlear bundle stimulation affects cochlear biomechanical nonlinearity," Hear. Res. **6**, 171–182.
Smoorenburg, G. E., and Linschoten, D. H. (**1978**). "A neurophysiological study on auditory frequency analysis of complex tones," in *Psychophysics and Physiology of Hearing*, edited by E. Evans (Academic, London).
Terhardt, E. (**1975**). "Influence of intensity on the pitch of complex tones," Acoustica **33**, 5.
Transcripts of the mid-Symposium Discussion Period (**1980**). Hear. Res. **2**, 581–587.
Weiss, T. F. (**1982**). "Bidirectional transduction in vertebrate hair cells: A mechanism for coupling mechanical and electrical processes," Hear. Res. **7**, 353–360.
Weiss, T. F. (**1984**). "Relation of receptor potentials of cochlear hair cells to spike discharge of cochlear neurons," Ann. Rev. Physiol. **46**, 247–259.
Wever, E. G. (**1949**). *Theory of Hearing* (Dover, New York), pp. 340–346.
Wilson, J. P., and Evans, E. F. (**1983**). "Some observations on the 'passive' mechanics of cat basilar membrane," in *Mechanisms of Hearing*, edited by W. Webster and L. Aitkin (Monash U. P., Australia).
Young, E. D., and Sachs, M. B. (**1979**). "Representation of steady-state vowels in the temporal aspects of the discharge patterns of populations of auditory nerve fibers," J. Acoust. Soc. Am. **60**, 1381–1403.